ÇUKUROVA UNIVERSITY
INSTITUTE OF NATURAL AND APPLIED SCIENCES

MSc THESIS

WAFAA S. A. ABUSAID

EFFECTS OF ELECTRIC FIELD ON THE PROPERTIES OF CARBON-BASED THIN FILMS DEPOSITED BY ELECTRON CYCLOTRON RESONANCE MICROWAVE PLASMA (ECR-MP) SYSTEM

DEPARTMENT OF PHYSICS

ADANA, 2019

ÇUKUROVA UNIVERSITY
INSTITUTE OF NATURAL AND APPLIED SCIENCES

EFFECTS OF ELECTRIC FIELD ON THE PROPERTIES OF CARBON-BASED THIN FILMS DEPOSITED BY ELECTRON CYCLOTRON RESONANCE MICROWAVE PLASMA (ECR-MP) SYSTEM

WAFAA S. A. ABUSAID

MSc THESIS

DEPARTMENT OF PHYSICS

We certify that the thesis titled above was reviewed and approved for the award of degree of the Master of Science by the board of jury on 30/07/2019.

……..	……	…….
Prof. Dr. Ramazan ESEN	Prof. Dr. Hamide KAVAK	Prof. Dr. Hülya METİN GÜBÜR
Supervisor	Member	Member

This MSc Thesis is written at the Physics Department of Institute of Natural and Applied Sciences of Çukurova University.
Registration No:

Prof. Dr. Mustafa GÖK
Director
Institute of Natural and Applied Sciences

This study was financially supported by Çukurova University Academic Research Projects Unit.
Project No: FYL-2018-11242

ABSTRACT

MSc. THESIS

EFFECTS OF ELECTRIC FIELD ON THE PROPERTIES OF CARBON-BASED THIN FILMS DEPOSITED BY ELECTRON CYCLOTRON RESONANCE MICROWAVE PLASMA (ECR-MP) SYSTEM

WAFAA S. A. ABUSAID

ÇUKUROVAUNIVERSITY
INSTITUTE OF NATURAL AND APPLIED SCIENCES
DEPARTMENT OF PHYSICS

Supervisor : Prof. Dr. Ramazan ESEN
Year: 2019, Pages: 79
Jury : Prof. Dr. Ramazan ESEN
: Prof. Dr. Hamide KAVAK
: Prof. Dr. Hülya METİN GÜBÜR

In this study, carbon-based semiconductor thin films were deposited on glass and silicon substrates by electron cyclotron resonance microwave plasma chemical vapor deposition (ECR-MP CVD) system. Methane (CH_4) gas was used as a carbon plasma source. Hydrogenated silicon- carbide thin-films (Si_xC_y: H) (taking substrate as Si source) obtained for the first time. The optical and structural properties of the produced films were measured by spectrophotometer, Raman spectroscopies, X-ray diffractometer and atomic force microscopy (AFM). An external electric field was applied to the plasma during deposition some of the films that will help in optimizing the deposition. The influences of the applied bias voltage on the film properties were investigated. The effects of the deposition pressure on optical properties were also discussed. The results indicate that the band gap energy increases with increasing the deposition pressure while it decreases as the applied voltage increases. The optical transmission ratio decreases in the presence of the electric field. C and H ions with different q/m ratios result in different C/H film regions. The biased deposited films were more crystalline and more ordered structure as compared to unbiased films.

Keywords: Carbon thin films, CH_4, ECR-MP CVD, Band gap energy

ÖZ

YÜKSEK LİSANS TEZİ

ELEKTRON SİKLOTRON REZONANS MİKRODALGA PLAZMA (ECR-MP) SİSTEMİ İLE ELEKTRİK ALANIN KARBON BAZLI YARIILETKEN İNCE FİLMLERİN ÖZELLİKLERİNE ETKİLERİ

WAFAA S. A. ABUSAID

ÇUKUROVA ÜNİVERSİTESİ
FEN BİLİMLERİ ENSTİTÜSÜ
FİZİK ANABİLİM DALI

Danışman : Prof. Dr. Ramazan ESEN
Yıl: 2019, Sayfa: 79
Jüri : Prof. Dr. Ramazan ESEN
: Prof. Dr. Hamide KAVAK
: Prof. Dr. Hülya METİN GÜBÜR

Bu çalışmada, karbon bazlı yarıiletken ince filmler cam ve silisyum alttabanlar üzerine Elektron Siklotron Rezonans Mikrodalga Plazma (ECR-MP) yöntemi ile depolandı. Plazma oluşumu için metan (CH_4) gazı kullanıldı. Hidrojenlenmiş silisyum karbür ince filmler (Si_xC_y: H) (silisyum kaynağı olarak substrate alınarak) ilk kez elde edilmiştir. Elde edilen filmlerin optiksel, yapısal ve yüzey özellikleri spektrofotometre, Raman spektroskopisi, X-ışınları kırınımı (XRD) yöntemi ve atomik kuvvet mikroskobu kullanılarak belirlendi. Bazı filmlerin depozisyonu sırasında, depolama optimizasyonuna yardımcı olması için, plazma üzerine dış elektrik alanı uygulanmıştır. Uygulanan ön gerilimin film özelliklerine etkisi incelenmiştir. Depozisyon basıncının optik özellikler üzerindeki etkileri de gözlenmiştir. Yasak enerji aralığının uygulanan gerilimin artarken azaldığını depolama basıncının artması ile arttığını sonuçlar göstermektedir. Elektrik alanın varlığında optik geçirgenlik oranı düşemektedir. Farklı yük oranları ile C ve H iyonları farklı C/H film bölgeleri ile sonuçlanmaktadır. Ön gerilim uygulanarak depolanmış filmler ön gerilim uygulanmamış filmlere kıyasla daha kristallize ve daha düzenli yapıya sahipolduğu gözlenmiştir.

Anahtar Kelimeler: Karbon ince film, CH_4, ECR-MP CVD, Yasak bant aralığı

ACKNOWLEDGMENT

This thesis would not have been possible without the help and support of my Supervisor Prof. Dr. Ramazan ESEN. I really consider myself as a lucky person for one reason that is being supervised by Prof. Dr. Ramazan ESEN. I thank him for his kind endless help, great patience, good mentoring and guidance in conducting and finishing my thesis. Prof. Dr. Ramazan ESEN inspired me with his great dedication and gave me the insights that sparked my passion to knowledge. I extend my sincere appreciation to the professors of the committee Prof. Dr. Hamide KAVAK and Prof. Dr. Hülya METİN GÜBÜR. I thank them for taking time to read and discuss my work. I am very grateful to all my professors in physics department at Çukurova University.

I am deeply thankful to Dr. Mehmet Esen for his collaboration in conducting my work experiments in the laboratories. I really admire Dr. Mehmet Esen who is distinguished and creative. I am also thankful to the research assistant Mrs. Merhan KILIÇ and Mr. Mehmet Selim ASLAN who provided me with all the help I needed. I would like to acknowledge my research group who is always with me during my work.

My sincere thanks go to Turkish government represented by Presidency for Turks Abroad and Related Communities (Yurtdışı Türkler ve Akraba Topluluklar Başkanlığı YTB) for their generous financial support. I am also grateful to my professors at Islamic University of Gaza who gave me their confidence and nominated me for the Turkish Scholarship. My deepest thanks to Dr. ZAHER NASSAR for his assistance, suggestions and caring for my work. Special thanks to Dr. Osama Elbelbessi who has been solving any problem I face in my computer throughout writing my thesis.

Finally, I must express my very profound gratitude to my family, especially my parents and my sister Ola, for enabling me to gain so much confidence, valuable feedback and sacrifices. Thanks a lot to my friends especially my best friend Mariam Abu Tailkh for providing me with unfailing support and continuous encouragement.

CONTENTS **PAGE**

ABSTRACT III
ÖZ IV
ACKNOWLEDGMENT V
CONTENTS VI
LIST OF TABLES VIII
LIST OF FIGURES X
SYMBOLS AND ABBREVIATIONS XIV
1. INTRODUCTION 1
2. LITERATURE REVIEW 5
3. MATERIAL AND METHOD 11
3.1. Material 11
3.1.1. Carbon-Based Materials 11
3.1.2. Diamond-Like Carbon (DLC): Properties and Applications 17
3.1.2.1 Automotive Engine Applications 17
3.1.2.2 DLC Coating on Cutting Tools and Hard Disks 18
3.1.2.3. Food and Beverage Applications 19
3.1.2.4 Biomedical Applications 20
3.1.3. Silicon Carbide (SiC): Properties and Applications 22
3.2. Method 23
3.2.1. Main Processes for Carbon Coating 23
3.2.1.1. Physical Vapor Deposition (PVD) Technique 23
3.2.1.2. Chemical Vapor Deposition (CVD) Technique 24
3.2.2. ECR Plasma Enhanced Film Deposition System 25
3.2.2.1. Major Components of ECR Plasma Sources 26
3.2.2.2 The Operating Principle of ECR Plasma Sources 33
3.2.2.3 The Advantages and Disadvantages of ECR Sources 33

3.2.3 Production of Carbon- Based Semiconductor Thin Films 34
3.3. Characterization of Thin Films 34
3.3.1. X-Ray Diffraction 35
3.3.2. Determination of Optical Properties of Films 36
3.3.2.1. Calculation of Absorption Coefficient 37
3.3.2.2 Direct and Indirect Band Gaps 42
3.3.2.3. Calculation of Forbidden Bandgap Energy 43
3.3.2.4. Calculation of Urbach Energy 44
3.3.3 Atomic Force Microscopy (AFM) 45
3.3.4 Raman Spectroscopy 48
4. RESULTS AND DISCUSSION 51
4.1 Optical Properties 54
4.1.1. Optical Properties of Carbon Thin Films Deposited on Glass Substrate Without Applying Any External Field 54
4.1.2. Optical Properties of Carbon Semiconductor Thin Films Deposited on Glass Substrate With Applying External Field 57
4.2. Raman Measurements 61
4.2.1. Results of Raman Spectroscopy for Carbon Thin Films Deposited on Glass Substrate 61
4.2.2. Results of Raman Spectroscopy for Carbon Thin Films Deposited on Silicon Substrate 63
4.3. XRD Results 65
4.4 AFM Results 66
5. CONCLUSION 69
REFERENCER ..... **Hata! Yer işareti tanımlanmamış.**
CURRICULUM VITAE 79

LIST OF TABLES **PAGE**

Table 4.1. Parameters for films deposited on glass substrate under different working pressure without any external field 53
Table 4.2. Parameters for films deposited on biased glass substrate with an external field 53
Table 4.3. Parameters for SiC films deposited onto Si substrate 54
Table 4.4. Thickness (d) of W-3, W-4 and W-5 thin films 56
Table 4.5. Band gap energy (Eg) of obtained thin films for 30 min at different values of working pressure 56
Table 4.6. Peak position, half-widths and intensity obtained from Raman measurements of samples W-9, W-10 and W-11 63
Table 4.7. Intensity, FWHM and grain size obtained from XRD analysis. 66

LIST OF FIGURES **PAGE**

Figure 3.1. The electronic configuration of carbon in the ground and excited state 11
Figure 3.2. Schematic representation of sp^3, sp^2 and sp^1 hybridized atoms 12
Figure 3.3. Allotropes of carbon: a. Diamond b. Graphite c. Amorphous carbon d. Spherical fullerene, C60 e. Ellipsoidal fullerene, C70 f. Tubular fullerene, SWCNT..... 13
Figure 3.4. Diamond..... 13
Figure 3.5. Graphite..... 14
Figure 3.6. Fullerene..... 14
Figure 3.7. Amorphous carbons 15
Figure 3.8. Ternary phase diagram of the amorphous carbon-hydrogen system.. 17
Figure 3.9. DLC-coated aluminum alloy piston 18
Figure 3.10. Hard disk architecture..... 19
Figure 3.11. The gas barrier mechanism of DLC coating on PET bottles. 20
Figure 3.12. The orthopedic screw with DLC coating screwings into bone..... 21
Figure 3.13. Orthodontic treatment..... 21
Figure 3.14. Silicon carbide abrasive rolls..... 22
Figure 3.15. Classification of coating processes..... 23
Figure 3.16. PVD process flow diagram..... 24
Figure 3.17. CVD process flow diagram 25
Figure 3.18. Plasma enhanced chemical vapor deposition (PECVD)..... 25
Figure 3.19. A schematic diagram of ECR-CVD system 26
Figure 3.20. Plasma gun..... 27
Figure 3.21. Reaction chamber 28
Figure 3.22. Inside of the vacuum chamber..... 28
Figure 3.23. Atom / Ion hybrid source..... 29
Figure 3.24 Gas flow-pressure control system..... 29

Figure 3.25. Gas valve 30
Figure 3.26. Turbo molecular pump system 31
Figure 3.27. CH_4 tube used in film production 32
Figure 3.28. Digram of Bragg's law 36
Figure 3.29. X-ray diffractometer 36
Figure 3.30. Perkin-Elmer UV/VIS Lamda 2S spectrophotometer 37
Figure 3.31. Absorption in a thin layer 38
Figure 3.32. Transmission of multilayer thin film 40
Figure 3.33. Schematic graph of energy against crystal momentum (or $\vec{k}$ vector) for a direct-bandgap semiconductor 43
Figure 3.34. Schematic graph of energy against crystal momentum (or $\vec{k}$ vector) for an indirect-bandgap semiconductor. 43
Figure 3.35. The change in the absorption coefficient of an amorphous semiconductor according to energy 45
Figure 3.36. A schematic diagram for the working principle of AFM 46
Figure 3.37. Different regions within the force curve 47
Figure 3.38. Different transitions involved in Raman spectra 49
Figure 3.39. Schematic plot showing Rayleigh scattering and Raman spectrum (+ve frequency for Stokes scattering and -ve frequency for anti-Stokes) 50
Figure 4.1. Image of deposition on Si substrates 52
Figure 4.2. Image of deposition on glass substrates 52
Figure 4.3. The transmittance spectra of six films produced at different working pressure of 45W microwave power. 55
Figure 4.5. Optical energy gap determination for carbon films with different working pressure. 57
Figure 4.6. The transmittance spectra of three thin films produced at the same working pressure 4.5×10^{-3} Torr and different applied voltage. 58

Figure 4.7. The absorption spectra of three thin films produced at different applied voltage 59
Figure 4.8. Optical energy gap determination for carbon films with different applied voltage. 60
Figure 4.9. Raman spectra of carbon thin films fabricated on the glass substrates at different bias voltage. 61
Figure 4.10. Raman spectra of carbon thin films deposited at different bias voltages: (a) unbiased (b) 150V (c) 155V and (d) 200 V..... 62
Figure 4.11. Raman spectra of SiC thin films grown on Si substrates..... 64
Figure 4.12. Raman measurements for two SiC thin films (a) no bias (b) with150 V bias voltage..... 64
Figure 4.13. XRD pattern for SiC thin films..... 65
Figure 4.14. AFM 3D images of carbon films (a), (b) unbiased (c), (d) biased 67

SYMBOLS AND ABBREVIATIONS

ECR-MP CVD	: Electron Cyclotron Resonance Microwave Plasma Chemical Vapor Deposition
PVD	: Physical Vapor Deposition
Si_xC_y:H	: Hydrogenated Silicon-Carbon Thin-Films
CNTs	: Carbon Nanotubes
DLC	: Diamond Like Carbon
XRD	: X-Ray Diffraction
AFM	: Atomic Force Microscope
IBD	: Ion Beam Deposition
SE	: Spectroscopic Ellipsometry

1. INTRODUCTION

Nanostructured materials have been a widespread subject over the past three decades. The importance of nanocrystalline materials is not associated with only the fact that these materials widen our understanding of structural and optical properties of crystals down to nanometer size, but also the fact that they present a prominent potential for wide applications in technology thanks to their unique properties (Andres et al. 1989).

Carbon is one of the most abundant and versatile elements in nature. It is known as a building block of life. The carbon atoms can bond together in different ways, forming many allotropes like graphite, diamond and amorphous carbon. This makes carbon an interesting material in many applications (Delhaes 2013). Carbon-based thin films have excellent characteristics like high stability, mechanical strength, low thermal expansion coefficient, non-chemical reaction and high thermal conductivity at room temperature. For these reasons, they are attractive materials for many electro-optical device applications, particularly photovoltaic solar cells (Charitidis and Materials 2010).

The first insulating carbon film was produced by Aisenberg and Chabot using the ion beam deposition (IBD) process. It was noticed that these carbon films had similar properties to natural diamond. In 1971, Aisenberg and Chabot named this material as ‘Diamond-Like Carbon’ (DLC) to describe the new form of amorphous carbon. During the past two decades, deep interest has been paid for using diamond-like carbon materials for coating because of their useful properties such as high mechanical hardness, low friction coefficient, chemical inertness, high wear resistance and high biocompatibility (Robertson and Reports 2002). The major advantage of DLC is that they can be grown at room temperature (Bewilogua, Hofmann, and Technology 2014; Dey et al. 2008). Diamond-like carbon coatings have a wide range of industrial applications to improve the performance of wear parts, especially in the automotive industry. Besides, DLC

films have widespread applications as protective coatings in hard disks and magnetic recording heads. They are also used as an anti-wear layer on cutting tools, razor blades and as an anti-reflective layer on sunglasses. DLC is a non-toxic material and has high level of biocompatibility which makes it suitable for use as surface coatings for in-body biomedical devices like stents, hip and dental implants.

Another very versatile group of carbon materials is silicon carbide (SiC). Silicon carbide (SiC) is considered as a promising coating material. It has recently attracted interest due to its outstanding physical and chemical properties, such as the wide band gap, high surface hardness, high thermal electronic conductivity, high-saturated electron velocity and large electrical breakdown field. SiC films find a variety of high frequency, high power, high temperature applications, as well as a corrosion-resistant coating (Lei et al. 2000; Sha, Wu, and Zhuge 2005).

Films have usually been grown by using various deposition methods, including ion beam assisted deposition chemical vapor deposition, pulsed laser deposition, sol-gel and magnetron sputtering. The properties of thin film are highly dependent on the deposition method, parameters and test conditions. Each method has its own advantages and disadvantages. One of these methods is the electron cyclotron resonance chemical vapor deposition method which appears to be very attractive thanks to its unique plasma properties like high electron temperature and high ionization rate. In comparison with other deposition methods, ECR-CVD process offers an attractive feature is that the energy of bombarding ions on the surface of the film can be controlled independently by applying a bias voltage to the substrates (Cui et al. 2001).

In this work, we are mainly concerned with electron cyclotron resonance chemical vapor deposition technique since the obtained thin films are grown by this technique. DLC and SiC thin films were deposited on glass and silicon substrates. Due to the importance of DLC and SiC semiconductor in technological applications, researchers have hard worked to investigate the properties of these

materials. Here, we investigate the optical and structural properties of these films using different characterization techniques such as spectrophotometer, Raman spectroscopy, atomic force microscopy (AFM) and X-ray diffractometer (XRD). The purpose of the present work was to study the influence of an external electric field on the structural and optical properties. A bias voltage was applied to the substrate during the deposition process. It is a critical parameter because it can provide additional energy to the produced film by attracting ions to bombard the substrate. The ion bombardment on the growth of film leads to variation in the film's properties (Yang et al. 2000). It was observed that the presence of the electric field strongly affects the band gap and optical transmission of the produced films. The results are consistent with each other and in agreement with previous studies.

2. LITERATURE REVIEW

Electron cyclotron resonance chemical vapor deposition method is used to deposit thin diamond-like carbon (DLC) films. Properties of these thin films were investigated. The effects of CH_4 plasma parameters on film deposition were also investigated. Thin films obtained by ions penetrating into the material. Films were found to be highly qualified and the energy was transferred at 16 eV/Å with a flux density same as that of radicals (Inaba et al. 2002).

Thin films of diamond like carbon (DLC) were deposited on silicon (111) substrates by ECR-CVD method using a plasma of Ar and CH_4 gases under different DC bias substrate ranging from 60V to 150V generated by applying RF (13.56 MHz) power. Deposited films were characterized by different techniques including contact angle measurement, atomic force microscopy (AFM), spectroscopic ellipsometry (SE), scanning electron microscopy (SEM), X-ray photoelectron spectroscopy (XPS) and Raman spectroscopy. The results showed that the film that had been grown at 100 V bias has optimized properties e.g. having a high contact angle (80) compared to the films deposited at other bias voltages (60 V and 150 V), high refractive index (2.26–2.17) over wide spectral range 400–1200 nm, high sp^3 /sp^2 ratio of carbon bonding, low roughness of 0.8 nm, (Dey et al. 2008).

Thin films of DLC were deposited on stainless silicon substrates and steel by a RF (13.56 MHz) magnetron sputtering technique. A gas mixture of Ar/CH_4 and a carbon target 99.99% were used. The films were analyzed by scanning electron microscopy SEM, Raman spectroscopy and infrared spectroscopy. The Raman intensity of the diamond and graphite peaks (I_D/I_G) rely on the proportion of CH_4 in the gas mixture. It was observed that there were sp^3 CH_2 symmetric and asymmetric at 2870 and 2960 cm^{-1}stretching peaks in IR spectroscopy analysis. These peaks were observed in diamond-like carbon DLC films and in diamond deposited at high CH_4 concentrations (Sanchez et al. 2000).

DLC films have been grown by pulsed DC discharge plasma chemical vapor deposition (CVD) using mixed gases of hydrogen and methane. From Raman analysis, increasement of carbon film graphitization was noticed at 40% of methane concentration. The white light photoconductivity at room temperature was about 20. When methane concentration was lower than 20%, the photoconductivity was not clear. ESR results indicate that when methane concentration decreased the density of electron spin was also decreased (Kawai et al. 2008).

Nanomechanical properties of hydrogenated amorphous carbon thin films were determined by nanoindentation method. Hydrogen amorphous carbon thin films were deposited onto silicon substrates by ECR-MPCVD system. The influence of negative bias voltage on these films was investigated by Raman spectroscopy. The results indicate that with increasing the applied voltage the intensity ratio (I_D/I_G) increased. Meanwhile, Young's modulus and hardness degree increased. Both the Young's modulus and the degree of hardness decreased as the indentation depth increased (Jian, Fang, and Chuu 2004).

CN_x: H films were deposited on silicon substrates in the temperature range of 700-950°C by chemical vapor deposition using ethylenediamine. Temperature effects on film properties was investigated. From the XRD pattern, it was found that films produced at 700°C and 800°C were amorphous. A wide XRD peak was observed at 25.6°C indicating that the films deposited at 900°C and 950°C had nano-crystalline structures. From XPS measurements, it was seen that N/C ratio decreased with increasing temperature but N-sp^2 C bonds increased. G peak position and I_D/I_G ratio were obtained from Raman measurements. As the temperature increased, the G peak shifted to higher values and the I_D/I_G ratio increased, which had been evaluated as a conversion to the nano-crystalline graphite structure. From FT-IR spectra it was confirmed that sp^2 and sp^3 bonds had been formed between carbon and nitrogen atoms to form CN_x:H films. It was found that the wear resistance hardly increased by elevating temperature and the sample produced at 900°C had higher wear resistance value than the sample produced at

950°C. Besides, these samples had longer wear life and lower friction coefficient of than those produced at lower temperatures. The structure of samples fabricated at a higher temperature was more compact and the surface roughness was larger because of the formation of nanocrystalline carbon nitride. In this study, the influence of the thickness on antiwear life was also investigated. It was observed that the thickest film had the longest wear life (Guo et al. 2011).

Carbon nitride films were synthesized by direct current radio frequency plasma using the chemical vapor deposition method. CH_4 and N_2 were used as a plasma source. The pressure was varied in the range of 2-20Pa. The CH_4/N_2 ratio was fixed in 1:1 and no external heating was applied. It was found that the N/C ratio increased as the pressure increased, but showed an exceptional decrease in the value of 5Pa. In addition, the hardness values of the films decreased with increasing pressure. It had been indicated that the deposition pressure increase as the nano-hardness reduce. The hardness values of films deposited at pressures below 10Pa were comparable to the hardness values of diamond-like carbon films. At higher pressure, films were converted to graphite structure and hardness values were found to be low. From FTIR and Raman results, it was confirmed that the fraction of C=N, C=C and C≡ N bonds increased and the fraction of C-N bonds decreased as the pressure increased. The growth rate rises with elevating the pressure of deposition because of the increasing in plasma density (Hao, Xu, and Liu 2005).

SiC thin-films were deposited by RF-magnetron sputtering method (RMS). In order to characterize the surface morphology of the films AFM had be used. The surface was observed to be uniform and very compact. From XRD analysis, it was revealed that the thin-films are amorphous. The square-resistance and the thickness were measured. The results show that the electronic mechanism of the SiC thin-films was short distance transition between the localized states in the temperature in the range of 25–250°C. The resistivity ranging from 2.4×10^{-3} to $4.4 \times$

10^{-3} Ω.cm and it had the same trend as electron excitation energy when the temperature is elevated, which confirms the electronic mechanism of thin-films and the trend of electron excitation energy versus the temperature (Zhou and Zheng 2007).

Diamond-like carbon (DLC) films have been deposited on Si substrate using a plasma CVD process under varying bias voltage. The effect of the applied voltage on mechanical, structural and tribological properties of the DLC films was investigated. The friction and wear properties in various environments (O_2, vacuum, N_2, dry-air and high moist air) have been measured. It was found that the sp3 C and H concentrations decreased when the substrate bias voltage increased from −1 to −3 kV. Hardness and internal stress also decreased while critical load increased. In addition, in the inert environments (N_2 or vacuum), the friction coefficient of the films had not been affected but a slight decrease in the reactive environments (O_2 or high moist air) had been observed by increasing the bias voltage of the substrate. In different environments, the wear resistance of the DLC films decreased as the substrate bias increased (Zhang et al. 2002).

Hydrogenated amorphous silicon carbide (a-$Si_{1-x}C_x$:H) films were deposited by the ECR-CVD system in different negative substrate bias voltage. The influences on the optical and structural properties were investigated. It was shown that the increase of the induced bias voltage from 220 to 2120V resulted in a slight increase of the carbon fraction x and obvious structural transformation. The FTIR results showed that H content increased at higher bias voltages. Room temperature visible photoluminescence (PL) with comparatively low efficiency could be observed and the number of Si dangling bonds was predicted to be small. When the bias voltage increased from 280 to 2120 V, slightly C-rich a-$Si_{1-x}C_x$:H films ($x > 0.5$) with larger optical gaps are observed. These films have sp^2 clusters formation. All the films leading to an increase in disorders as the bias voltage is increased (Cui et al. 2001).

Amorphous silicon carbide (a-SiC) films, was prepared as insulating coatings for implantable microelectrodes, using PECVD process. These films were deposited on metal wire and Si wafers to measure electrical leakage through the coating. Over a ±5V bias leakage currents were found to be low. The electronic resistivity of a-SiC was $3x10^{13}\Omega\cdot m$. Dissolution rates of a-SiC at 37 and 90°C were obtained by changing the infrared absorption band intensities and compared with those of silicon nitride fabricated using (LPCVD) process. The silicon nitride films had a dissolution rate of 2nm/h and 0.4 nm/day at 90 and 37°C, respectively, whereas the dissolution rates of a-SiC films were 0.1 nm/h at 90°C but at 37°C there was not any dissolution. Biocompatibility was determined from implantation a-SiC-coated quartz discs in the sub-cutaneous space of the New Zealand White rabbit. Amorphous SiC-coated microelectrodes were implanted for periods up to 150 days. The silicon nitride was found to be less stable in physiological saline than a-SiC. Overall, a-SiC films have desired properties as hermetic coatings on chronically implantable microelectrodes (Cogan et al. 2003).

The influence of the deposition pressure on the photoelectronic and microstructure properties of the hydrogenated silicon thin films deposited using (PECVD) were investigated. It was found that the bandgap increased with the increase of the deposition pressure. Meanwhile, as the deposition pressure rises from 100Pa to 500Pa, the crystalline volume fraction (X_C) reduces from 70% to 61%. In addition, The hydrogen content in the nc-Si:H films were increased by increasing the pressure from 5.5% to 11%.. Raman spectra showed that the increase in the pressure resulted in reduction of the volume fraction. The photosensitivity decreased from more than ~103 to ~102 (Karthik, Himaja, and Singh 2014).

Antimony selenide (Sb_2Se_3) thin films were deposited using RF magnetron sputtering onto glass substrates. The deposition occurred at room temperature under different working pressures in the range of (0.3-10)Pa. It was noticed that the working pressure has had a strong effect on the morphologies and microstructure.

Besides, the deposition pressure had a high relation with the growth orientation of films. At high pressures $(Sb_4Se_6)_n$ were found to be easier to grow disposed to [hk1] orientation, whereas the Sb_2Se_3 films had [hk0] orientation inclination at 0.3Pa and 2Pa. As anticipated, the films grown at higher pressures displayed better conductivity and the highest photocurrent. The solar cells were fabricated with a superstrate structure and high efficiency of 0.79% (Liang et al. 2019).

Al/p-Si/C_3N_4/Au Schottky diodes were produced by sol-gel spin process. The properties of current and voltage for Schottky diodes were investigated in darkness and under various light intensities. As the light intensity increases, the photocurrent values of the diodes increase. It was found that the photocurrent, conductivity and capacitance values were dependent on transient light. Photocurrent, conductivity and capacitance values have been increased with the Schottky diodes illumination and they return to their initial values when the illumination is turned off (Gupta et al. 2014).

3. MATERIAL AND METHOD

3.1. Material

3.1.1. Carbon-Based Materials

Carbon-based materials date centuries back in their synthesis and applications. A whole universe is involved with different crystallographic structures, such as natural and synthetic diamond, different modification of graphite, fullerene, carbon fibers, and their composites. The reducing of sample size in the range of a few nanometers has received growing interest and an awakening of the field in the last few years (Fecht and Brühne 2016).

Carbon, the 6th element in the periodic table is found almost everywhere. Carbon is a basic building block of all living organisms. The importance of carbon is primarily due to its ability of forming numerous strong bonds with itself and with other element bonds. The electronic configuration of carbon in the ground and the excited state is shown in Figure 3.1.

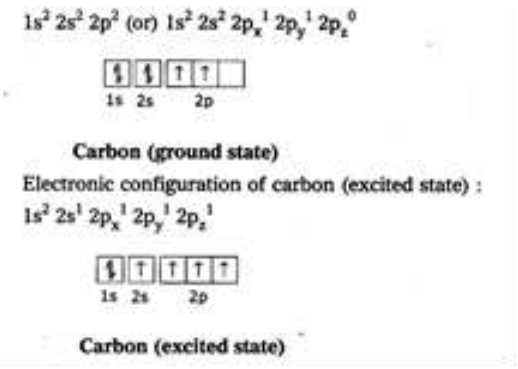

Figure 3.1. The electronic configuration of carbon in the ground and excited state

There is a possibility of three different mixing ways to form three types of hybridizations, namely sp^1, sp^2 and sp^3, as shown in Figure 3.2. In the sp^3 configuration, the 2s orbital and three 2p orbitals are hybridized to form four energy equivalent sp^3 hybrid orbitals arranged in a tetrahedral structure with an angle of 109.5^0. These orbits form strong C–C σ bonds with adjacent atoms. The sp^2 hybridization explains the trigonal planar structure of orbits where the bond angle is 1200^0. In this hybridization, the 2s orbital and two of the 2p orbitals hybridize to form three identical sp^2 hybrid orbitals. The third 2p orbital, known as a π orbital, remains unchanged and is perpendicular to the plane of the three sp^2 orbits at a higher energy level. In its bonding, strong σ bonds are formed by overlapping two sp^2 orbits and there is a relatively weaker π bond that takes place between unhybridized 2p orbitals. Sp^2 bonding in carbon is usually depicted as a C=C double bond which is made up of σ bond and π bond. However, Sp^1 bonding is a C≡C triple bond. A single σ bond is formed by the two equivalent sp hybridized orbits and two π bond occur due to the two π orbits (Yeo 2017).

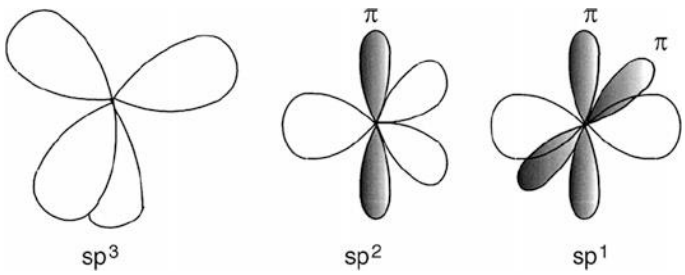

Figure 3.2. Schematic representation of sp^3, sp^2 and sp^1 hybridized atoms (Robertson and Reports 2002).

Carbon can form many allotropes with encouraging properties in a large spectrum of applications. The most common allotropes are diamond, graphite, fullerene and amorphous carbon. Figure 3.3 shows the crystallographic structures of these allotropes.

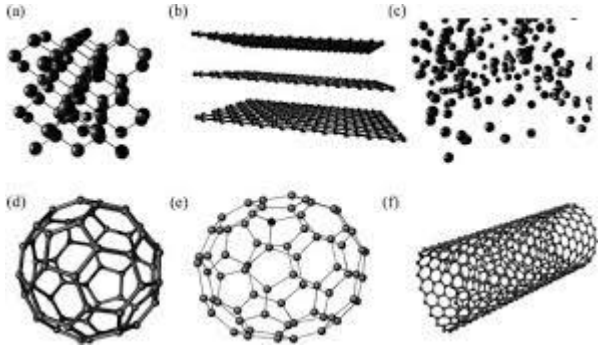

Figure 3.3. Allotropes of carbon: **a.** Diamond **b.** Graphite **c.** Amorphous carbon **d.** Spherical fullerene, C60 **e.** Ellipsoidal fullerene, C70 **f.** Tubular fullerene, SWCNT (Ren, Lan, and Wang 2012).

1) Diamond

Figure 3.4. Diamond

In diamond, the carbon atoms (sp^3 hybridized) are arranged in a tetrahedral lattice. Natural diamonds are formed at a pressure of 5-6 Gpa and temperatures ranging between 900-1400°C (Pal'Yanov et al. 1999). Diamond is famous for its extreme hardness originating from the strong carbon-carbon covalent bonds. It is an electrical insulator and thermal conductor. Diamond is fundamentally used in polishing tools, industrial cutting and is used as a gemstone (Ren, Lan, and Wang 2012).

2) Graphite

Figure 3.5. Graphite

Graphite has a planar structure of carbon atoms stacked in layers. In each layer, the carbon atoms are bonded together in a hexagonal arrangement, which makes it one of the softest natural materials. The carbon atoms in each graphite layer are sp^2 hybridized, the layers are connected to each other by a weakly van der Waals force. Graphite is a semi-metal within the layer, with less conductivity in the other direction. It is mainly used in industry as a lubrication (Ren, Lan, and Wang 2012).

3) Fullerene

Figure 3.6. Fullerene

The atoms in fullerene are arranged in pentagons and hexagons to form the shape of a hollow sphere, ellipsoid or tube. There are many types of fullerenes including buckyball clusters, nanotubes, mega tubes and nano onions (Mohan Gokhale and Ravindra Somani 2015).

Fullerenes that are in the form of a tube are referred to as carbon nanotubes CNTs. The carbon atoms in a CNT are connected in a curved sheet that forms a hollow cylinder with diameters in nanometers, while their length can reach several microns even millimeters.

Fullerene has low density (1.65 g/cc). It can undergo diverse reactions such as reduction, oxidation, hydrogenation, radical reaction and so on. Fullerenes are susceptive to decomposition in the presence of light and oxygen (Mohan Gokhale and Ravindra Somani 2015).

4) Amorphous carbon

Figure 3.7. Amorphous carbons

Amorphous carbons which cover a large category of carbon allotropes. The atoms or molecules of amorphous carbons are not arranged in a regular geometric pattern. Amorphous carbons can have any mixture of sp^3, sp^2 and even sp^1 sites. So their structures are intermediate between graphite (completely sp^2) and diamond (completely sp^3).They display some characteristics of diamond and graphite, relying on the ratio of sp^2/sp^3 (Yeo 2017).

The existence of hydrogen during deposition process forms a hydrogenated amorphous carbon. Robertson classified the hydrogenated amorphous carbons into four groups as the following:

(1) a-C: H films with H content of 40–60% that are called polymer-like a-C: H (PLCH) films. The hardness and density of these films are low, have a band gap in the range of (2-4) eV, the Sp^3 bond ratio is up to 70%. They are generally deposited at low bias voltage using plasma enhanced chemical vapor deposition (PECVD) (Robertson and Reports 2002).

(2) a-C: H films with 20–40% H content which usually termed as diamond-like a-C: H (DLCH). Sp^3 C-C bonding in (DLCH) is comparatively higher than (PLCH) films, therefore they have better mechanical properties. Their band gap ranges from 1eV to 2eV. They are usually deposited by (PECVD) or electron cyclotron resonance (ECR) or reactive sputtering (Durand-Drouhin, Lejeune, and Benlahsen 2002).

(3) Tetrahedral a-C: H (ta-C: H) is a specific type of hydrogenated DLC films. The C-C sp^3 content can be raised at a constant H content. Hydrogen content is about 25–30% whereas sp^3 C-C bonding reaches to 70% and the density is up to 2.4 g/cm^3. Their optical gap is about 2.4 eV. These films are deposited by high-density plasma sources such as electron cyclotron wave resonance (ECWR) and plasma beam source (PBS) (Kleinsorge et al. 2001).

(4) a-C: H films with 10–20% H content have a high sp^2 bonding and a band gap of 1eV. These films are known as graphite-like a-C: H (GLCH) and can be deposited by magnetron sputtering or by PECVD (Casiraghi, Ferrari, and Robertson 2005).

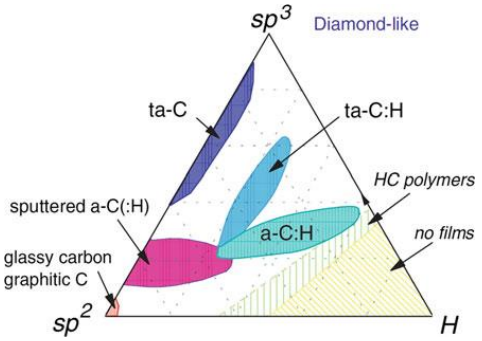

Figure 3.8. Ternary phase diagram of the amorphous carbon-hydrogen system.

3.1.2. Diamond-Like Carbon (DLC): Properties and Applications

Diamond-like carbon (DLC) was first deposited by Aisenberg and Chabot in 1971 with an ion beam. Their electrical, chemical, mechanical and optical properties are similar to diamond. Over the last decade, DLC has been actively studied in the field of material engineering. It has range of uses in surface coating due to its outstanding properties which can be listed as (1) high hardness (2) smooth surface (3) wear resistance (4) thermal conductivity (5) electrical insulation (6) good adhesion to the substrate (7) high chemical inertness (8) low friction coefficient (9) transparency over long wavelength region. The properties of DLC coatings can be tailored by manipulating the bonding environment between sp^3 and sp^2 hybridized carbon atoms and their relative contents. In DLC, the sp^3 hybridized carbon (diamond) which is responsible for excellent mechanical properties, is irregularly mixed with the sp^2 carbon (graphite) and therefore justifies the name, diamond-like carbon (Paul, Bhar, and Pal 2010).

3.1.2.1 Automotive Engine Applications

Diamond-like carbon (DLC) coatings are increasingly being used in the automotive industry to reduce fuel consumption and CO_2 emissions by reducing friction and wear in the sliding parts of automotive engines. These coatings have

harmless nature to the human body because they consist mainly of carbon (Kano 2015).

Al alloy before coating **After DLC coating**

Figure 3.9. DLC-coated aluminum alloy piston

3.1.2.2 DLC Coating on Cutting Tools and Hard Disks

Tool manufacturers have a wide option of coating materials, from traditional coating to more recent multilayer coatings. Carbon-based materials, carbides and nitrides are most commonly used coating films in tool manufactures. DLC films have proved to be excellent tool coatings for non-metal materials and composite materials. The main inconvenient of DLC coating on cutting tools is the adhesion of the film during the cutting process (FOLEA, ROMAN, and LUPULESCU 2010).

Diamond-like carbon films form a critical protective layer on magnetic hard disks in which the information is stored. Since the DLC films provide wear and corrosion protection to the magnetic layers. Decreasing the film thickness decreases its hardness that may be expected to decrease the probability of corrosion (Schmuki 2001).

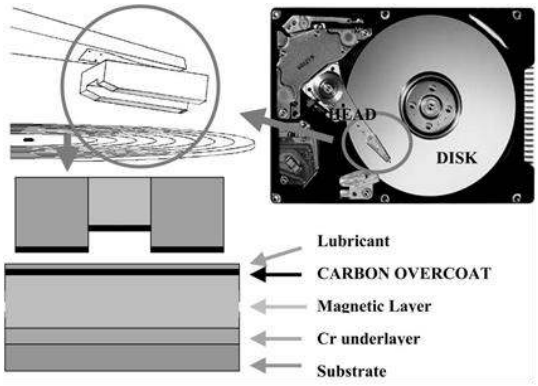

Figure 3.10. Hard disk architecture

3.1.2.3. Food and Beverage Applications

The use of plastic vessels in the food and beverage market has dramatically increased. PET bottles have gradually replaced glass bottles and metal cans because they are lightweight, unbreakable and flexible packaging material. Recently, PET bottles coated with DLC to provide the following main advantages:

- Gas barrier properties of DLC films prevent oxygen and carbon dioxide passing through the bottles.
- UV barrier increases the absorbance of ultraviolet ray.
- Chemical inertness: chemical stability with no interaction with contents.
- Recyclability: no obstacle to the recycling process for PET bottles.
- DLC coating increases the shelf life of some soft drinks from 10 weeks to 44-45 weeks (Shirakura et al. 2006; Robertson 2005).

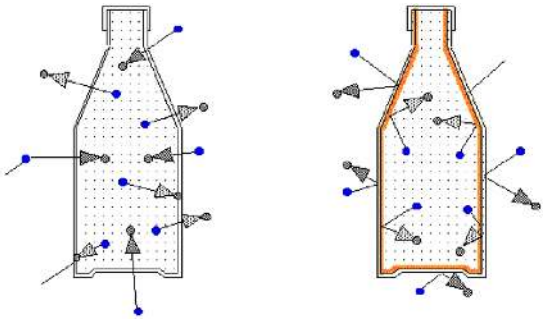

Figure 3.11. The gas barrier mechanism of DLC coating on PET bottles.

3.1.2.4 Biomedical Applications

Diamond-like carbon (DLC) is considered as a versatile biomaterial that finds many biomedical applications, such as cardiovascular, orthopedic surgery and dental implants (Gotzmann et al. 2017).

DLC materials are essential for cardiovascular implantable devices especially intravenous stents. They can prevent the adhesion and activation of platelets and promote the adsorption of albumin (Maegawa et al. 2016).

Silver nanoparticle (Ag NP) doped DLC is efficient for antibacterial coating applications (Schwarz et al. 2011). Lately, a new type of antibacterial bandage is proposed where Ag: DLC coated synthetic silk tissue is utilized as a building block (Schwarz et al. 2011).

DLC/metal nanoparticles are also promising for cancer treatment through photo-thermal therapy (PTT) in which photon energy is converted into heat to kill cancerous cells (Huang and El-Sayed 2011). In the last few years, DLC coating has been evaluated as a growth substrate for neurons cells which is quite interesting (Hopper et al. 2016).

DLC film has attracted interest regarding its use in orthopedic applications. DLC coatings on metals are preferred for hip and knee replacement. As compared to the uncoated metals, metals coated with DLC have found to offer lower wear rate and corrosion. Besides, they reduce the release of metallic ions into the body (Tyagi and Banerjee 2017).

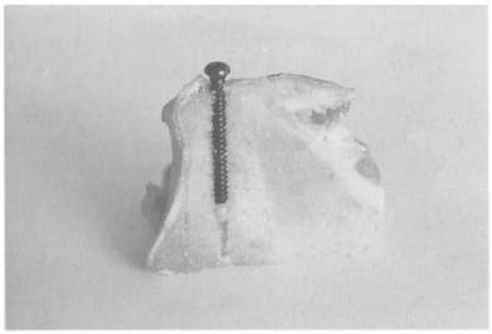

Figure 3.12. The orthopedic screw with DLC coating screwing into bone

DLC-coating process plays an important role in reducing the frictional force between the bracket and the wire during orthodontic tooth movement, therefore the efficiency of tooth movement can be improved (Muguruma et al. 2011).

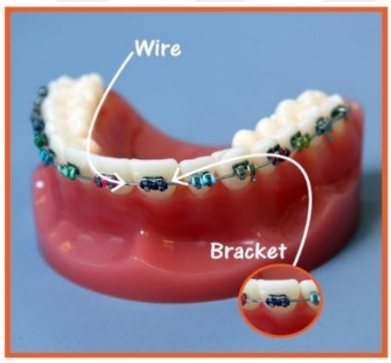

Figure 3.13. Orthodontic treatment

DLC coatings are also being applied to contact lenses to reduce biofilm formation (Roy 2017). The efficiency and radiation stability of silicon solar cells (SCs) can be markedly enhanced using the deposition of DLC films that meet the requirements of optimum antireflection and protection of SCs simultaneously (Litovchenko, Klyui, and cells 2001).

3.1.3. Silicon Carbide (SiC): Properties and Applications

Silicon carbide (SiC) has played an essential role in semiconductor device technology. In 1824, Jons Jacob Berzelius supposed that there was a chemical bond between silicon and carbon in one of the samples he had produced, he was the first person who synthesized SiC (Brezeanu 2005). SiC was used as a semiconductor material by Marconi Company for the first time in 1907 (Harris 1995). Silicon carbide has outline characteristics like high elastic modulus, low density, high thermal conductivity, excellent thermal shock resistance, superior hardness and corrosion resistance. These characteristics making it appropriate for applications in optoelectronic devices and microelectronic such as temperature sensors, phototransistors solar cells and light emitting diodes (Stamate 2001; Schmidt et al. 2005). SiC is also used as abrasive materials, It has been produced abrasive products like grinding wheels over the last century (Matějka et al. 2010). Silicon carbide antireflection (SiC AR) coatings improve the solar cell efficiency over 1.3 times. The improvement is connected with reducing the reflection losses (Klyui et al. 2002).

Figure 3.14. Silicon Carbide Abrasive Rolls

3.2. Methods

3.2.1. Main Processes for Carbon Coating

During the last decades, the methods of carbon coating have increased significantly. Coating processes and deposition technologies are changing rapidly to keep pace with developed film materials and applications. Figure 3.15 summarizes the classification of coating processes.

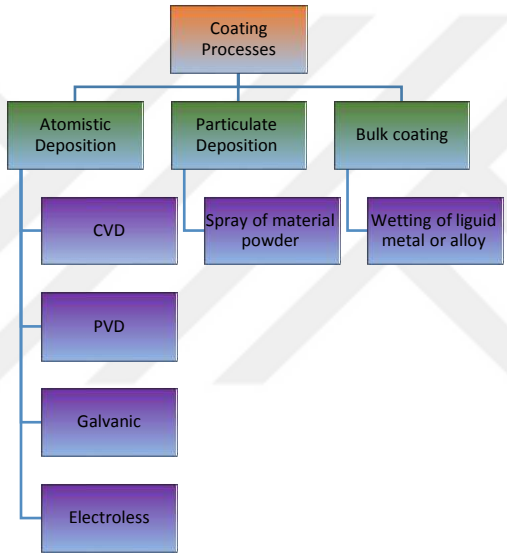

Figure 3.15. Classification of coating processes

3.2.1.1. Physical Vapor Deposition (PVD) Technique

In general, the PVD process is performed under vacuum circumstances. It is a molecular/atomistic deposition technique in which the target material is vaporized from liquid or solid source. The vaporized particles pass through a low-pressure gaseous or vacuum environment in the form of a vapor to reach the substrate and start condensing onto its surface to generate thin films. Physical vapor deposition technique is used to deposit films of thicknesses ranging from few

nanometers to few micrometers. The technique can also be used to form very thick deposits, graded composition deposits and multilayer coatings (Mattox 2010).

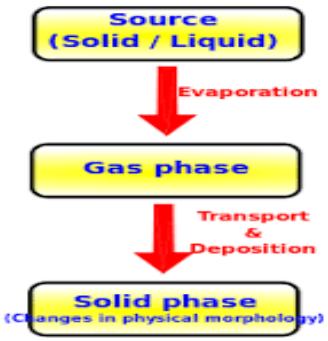

Figure 3.16. PVD Process flow diagram

3.2.1.2. Chemical Vapor Deposition (CVD) Technique

The CVD process involves depositing a solid material from a gaseous phase; this is achieved by means of a chemical reaction. Gaseous reactants admitted into a reactor are thermally activated near or on heated surface of a substrate leading to a chemical reaction of the type:

$A_{(g)} + B_{(g)} \xrightarrow{T/P} C + D$

A and B are gaseous reactants entering the reactor.

C: Solid material which depositing onto the substrate surface

D: Gaseous product leaving the reactor

T: Temperature P: Pressure (The reaction conditions inside the reactor)

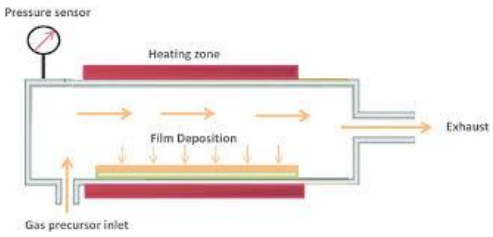

Figure 3.17. CVD Process flow diagram

Actually, CVD process has many types; however, this study will only explain the worthy one of them. Plasma enhanced chemical vapor deposition (PECVD) is a technique that employs plasma to provide the need energy for the chemical reaction as well as to allow coating to take place at a low temperature. One of the important advantages of the PECVD system is that the deposition can occur in large areas at relatively low temperatures. Moreover, the ion current and ion energy can be controlled separately. On the other hand, one of its meaningful disadvantages is that the film has low purity. Besides, this technique is usually more expensive than other techniques (Jameel and Applications 2015).

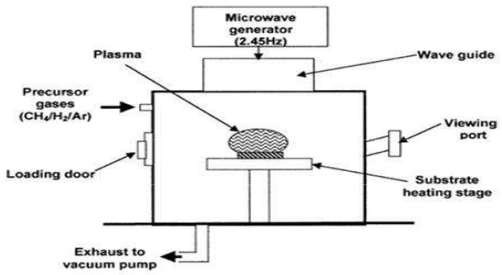

Figure 3.18. Plasma enhanced chemical vapor deposition (PECVD) (Choy, 2003).

3.2.2. ECR Plasma Enhanced Film Deposition System

Electron cyclotron resonance plasma source is a multi-purpose source which can easily produce either atoms or ions and finds uses in a wide range of high and ultra-high vacuum (HV/UHV) applications. The performance of the plasma source has an important affect in various fields of research and technology.

The ECR sources were first studied in the 1960s by Miller et al as a system for spacecraft propulsion. After that, many studies used ECR in fusion research. In addition, ECR based ion sources were developed due to their high plasma density at low pressure. In accelerator laboratories, ECR ion sources had become the most common ion sources for heavy ion production. They are used in medical and industrial applications such as cancer treatment, plasma propulsion and ion beam lithography.

3.2.2.1. Major Components of ECR Plasma Sources

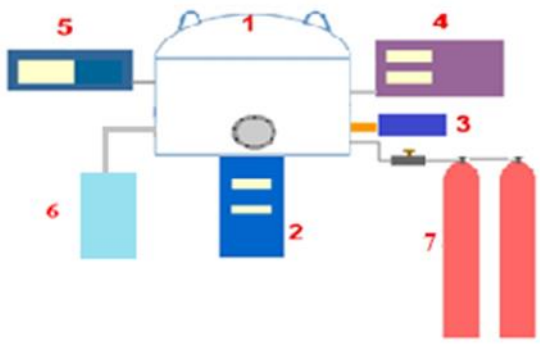

Figure 3.19. A schematic diagram of ECR-CVD system

ECR system consists of the following basic components:

1. Reaction chamber
2. Turbo molecular pump and rotary pump
3. Plasma source
4. Microwave source and extraction voltage source
5. Gas flow indicator
6. Cooling Unit
7. Methane Tubes

1. Microwave magnetron (Plasma source)

Microwave magnetron is a high-powered vacuum tube which uses the interaction of a magnetic field with a stream of electrons to generate microwaves. As shown in Figure 3.22, half of the plasma gun inside the chamber and the other half is outside. Microwaves with a frequency of 2.45GHz are generated by the microwave magnetron. High purity methane gas can be set by using MKS mass flow controller is introduced into the resonance chamber. The diameter of output ion beam is 3cm.

Figure 3.20. Plasma gun

2. Reaction chamber

Figure 3.21. Reaction chamber

Figure 3.22. Inside of the vacuum chamber

Reaction chamber is made of cylindrical 304 stainless steel (28 cm in height, 39 cm in diameter). There are two thermal pressure gauges, 1 ionization gauge, 1 observation window, 1 valve and substrate holder. An SRS GW-100F pressure sensor fitted into the end of the ion gauge, sometimes pressure is controlled from it depending on the pressure range. A mirror is placed inside the chamber for observing the plasma more comfortably, it can be observed from the chamber window.

3. Atom / Ion Hybrid Source

Figure 3.23. Atom / Ion Hybrid Source

The power system, current and voltage values can be adjusted with atom/ion hybrid source. The dial marked "power" controls the power, it is varied in the range 25-150 Watt. Voltage values are displaced in the middle panel meter. The ion current is shown in the adjacent panel meter, it can vary between 0-1mA. The ion energy is set to maximum value (2 keV). The independent control of current and ion energy is not possible, but it could be achieved if a bias voltage were to be applied to substrates.

4. Gas Flow-Pressure Control System

Figure 3.24. Gas Flow-Pressure Control System

Gas flow-pressure control system controls the pressure and the flow rate of a gas. There are 4 channel flow and one channel pressure. The MKS 1179A gas flow control system is available with full scale ranges from 10 sccm to 20 slm for precise and repeatable flow measurement and control. This system provides fast, repeatable flow control to as low as 0.2 sccm. It can also be used as a pressure controller when connected to a suitable pressure transducer.

Figure 3.25. Gas valve

The gas valve is shown in Figure 3.25 associated with a metal seal. It has a moving piston with a connected flat sapphire base. There is neither friction nor adhesion in the metal seal. Operating pressure ranges from atmospheric pressure to 10^{-11} Torr. It can withstand temperature up to 450C (Kurt J. LESKER, 1954). The pressure can be easily adjusted by adjusting the amount of gas introducing into the reaction chamber using the precision gas valve. Before reaching this valve reaction gases passes other two valves in series; one is rough valve other one is ten turns precise valve.

3. Turbo molecular Pump System

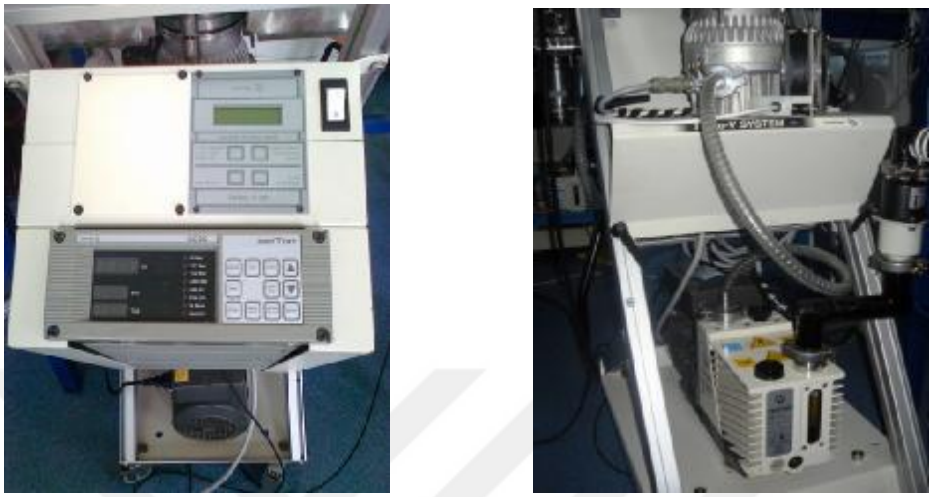

Figure 3.26. Turbo molecular Pump System

Before processing, reaction chamber is pumped down to a base pressure of 10^{-7} Torr with Varian 301 (350 L/s) turbo-pump and DS302 (15 m^3/h) rotary pump. Rotation speed is 56 revolution per minute (rpm).

Pumping speed:

8s CF or ISO 160: N 2: 280 1 / s He: 230 1 / s; H2: 210 1 / s

6/CF or ISO 100: N 2 = 250 1 / s, He = 220 1 / s, H2 = 200 1 / s

Compression ratio;

N2:> 2x108; H: 1x105; H2: 2x104.

(http://cires.colorado.edu/jimenez-group/QAMSRResources/Docs/V301.pdf)

4. Cooling system

Figure 3.27 Cooling system

During the deposition, cooling system is working to avoid the overheating of the microwave source. Cooling process is performed while the circulating of the cooled pure water in the ECR plasma source.

5. Methane Tube

Figure 3.27. CH_4 tube used in film production

Methane gas is obtained from the methane (CH_4) tube to the reaction chamber for producing carbon-based thin film.

5. Extraction system

The plasma ion source is fitted with dual extraction grids. The one is contact with the plasma is called the screen or anode grid, has a positive voltage applied to it and regulate the ion energy. The outer grid is called the extractor and has a negative voltage applied to it. We used one positive voltage for extraction and ion energy control.

3.2.2.2 The Operating Principle of ECR Plasma Sources

As the microwaves and the neutral gas are injected to the plasma chamber the ionization starts. A plasma is excited in the chamber and the microwaves absorbed. Free electrons moving on helical orbits are always present in the plasma chamber. When an external rapidly changing electric field E_{ext} is generated by the microwaves, free electrons can gain energy, if their gyration frequency ω_{ce} equals the microwave frequency m_e

ω_{RF} i.e.

$$\omega_{ce} = \frac{eB}{m} = \omega_{RF}$$

where B is the magnetic field. This is called electron cyclotron resonance.

The created plasma is further confined in the magnetic field to produce highly charged ions. Ions are extracted from the plasma chamber with the aid of high voltage to the extraction area.

3.2.2.3 The advantages and Disadvantages of ECR Sources

ECR system has positive and negative aspects. The main advantages of using this method can be listed as (1) high stability (2) high ionization efficiency (3) high plasma density (4) high degree of dissociation of molecules at low temperatures (Lee et al. 2015). However, it is important to know that ECR method has some drawbacks particularly, long conditioning times, slow deposition rate

high power consumption, high cost and complex technology for magnets, cooling systems and microwave components.

3.2.3 Production of Carbon- Based Semiconductor Thin Films

The first stage is cleaning the glass substrate. Clean slides prevent contamination of the sample allow for correct deposition of materials. The primary function of this method is to provide a strategy to remove everything from a glass substrate surface. Important processes for cleaning the glass substrate are as follows: (1) Preparing a bath of soapy water. Using a lint-free wipe to gently rub the surface cleaning of dirt and residues, then rinsing thoroughly in DI water (2) Putting the glass substrates into the washing acid for a while. For extra clean surfaces, soak for 24 hours. Then rinsing thoroughly in DI water (4) cleaning with methyl alcohol for 15min at room temperature. (5) Finally drying by nitrogen blowing. After cleaning the substrate, the cleaned substrate is placed on the substrate's holder. The holder is introduced into the chamber, in the front of the plasma source so that the ion beam is incident on the glass then covering the deposition chamber tightly. The vacuum pump is switched on after making sure that the valve on the reaction chamber is closed. The system pressure is monitored from the pressure gauge; the pressure is increased by introducing methane gas into the medium. Ion energy is adjustable about 0-2 keV. The gas flow is gradually increased to ignite the plasma. When plasma is obtained, it is waited for 2-5 minutes to stabilize the welding temperature. A shutter is opened to start the deposition. When the deposition process finishes, the system is turned off.

3.3. Characterization of Thin Films

Measurement of thin film properties is irreplaceable for the study of thin film materials. The chemical composition, crystalline structure, optical properties, electrical properties, and mechanical properties must be considered in thin films evaluation.

3.3.1. X-Ray Diffraction

X-ray diffraction (XRD) is a technique mainly used to identify the phase of crystalline materials, it can give information about the structure of crystals from the diffraction pattern generated by X-rays. The XRD patterns depend on the wavelengths and crystal structures; they are composed of a series of concentric rings. Each ring represents the diffraction produced from a group of the crystal planes (Kittel 2005). From the X-ray diffraction patterns, the average spacing between layers (rows of atoms), the orientation of the single crystal or grain, the crystal structure of an unknown material, the size, shape and internal stress of small crystalline regions can be determined.

Bragg's Law

William Lawrence Bragg offered an imagination of the light diffracted from crystals. He supposed that the incident light is reflected specularly[1] from the parallel atomic planes. The diffracted light is observed when the beams, which reflected from the atomic planes, are interfered constructively. The scattering using X-ray is elastic since the energy of X-ray does not change.

Assuming parallel atomic planes in the crystal spaced d apart, the path difference for the beams reflected from the successive planes is $2d \sin\theta$. Constructive interference takes place when the path difference equals an integer number n of the wavelength λ, the constructive interference condition is

$$2d \sin \theta = n\lambda \qquad (3.1)$$

which is called Bragg's law and it can be satisfied only if $\lambda \leq 2d$ (Kittel 2005).

[1] A specular reflection (mirror like reflection) is a reflection in which the angle of incidence and the angle of reflection are equal.

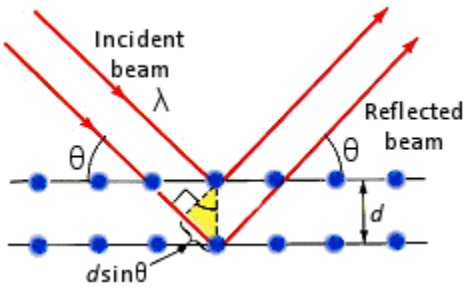

Figure 3.28. Diagram of Bragg's law

Figure 3.29. X-ray diffractometer

In X-ray diffractometer, the detector moves in a circle around the sample and its position is recorded as the angle (2θ). It records the number of X-rays observed at each angle 2θ. X-rays have wavelengths of the order of the atomic spacing. Therefore, X-rays are needed for examining the atomic lattice of crystals.

3.3.2. Determination of Optical Properties of Films

The extensive optical properties of solids can be classified into a few general phenomena. The simplest ones are reflection, absorption and transmission. We can quantify the optical phenomena by a group of parameters. Each parameter determines a property of the optical medium at the macroscopic level. Reflectivity (R), which is the coefficient of reflection, describes the reflection at the medium surface. It can be defined as the ratio between the reflected power and the incident power. The transmission is described by the transmissivity (T) (the coefficient of

transmission) which is defined as the ratio between the transmitted power and the power of the incident beam. According to the law of energy conservation we have

$$R + T = 1 \quad (3.2)$$

These measurements are determined by using Perkin-Elmer UV/VIS Lamda 2S spectrophotometer, with a wavelength range of 190 - 1100 nm. From the obtained transmission and absorption curves, absorption coefficient, energy band spacing, film thickness, Urbach energy, refractive index, oscillator energy, dielectric constants can be calculated.

Figure 3.30. Perkin-Elmer UV/VIS Lamda 2S spectrophotometer

3.3.2.1. Calculation of Absorption Coefficient

When a material with thickness (x) is shined by a monochromatic light beam with initial intensity (I_0) part of the incident light passes through the medium with intensity, while the rest light interacts with the material through reflection, absorption, or scattering. Neglecting the reflectance and scattering, the decrease in the intensity (dI) through an element of thickness (dx) is given by

$$dI = - \alpha I_0 \, dx \quad (3.3)$$

$$\alpha = -\frac{\Delta I}{I_0 \Delta x} \tag{3.4}$$

Here, (α) is the absorption coefficient, which quantifies the absorption of light during its propagation through the optical material. It is defined as the fraction of beam power that is absorbed by the medium per unit length.

$$\frac{dI}{I_0} = -\alpha dx \tag{3.5}$$

Equation 3.5 can be integrated to give the intensity through the total thickness(x)

$$\int_{I_0}^{I_T} \frac{dI}{I_0} = -\alpha \int_0^x dx \tag{3.6}$$

$$\ln\left(\frac{I_T}{I_0}\right) = -\alpha x \tag{3.7}$$

$$I_T = I_0 e^{-\alpha x} \tag{3.8}$$

$$I_T = I_0 e^{-\alpha x} \tag{3.9}$$

where I_0 is the intensity at x = 0.

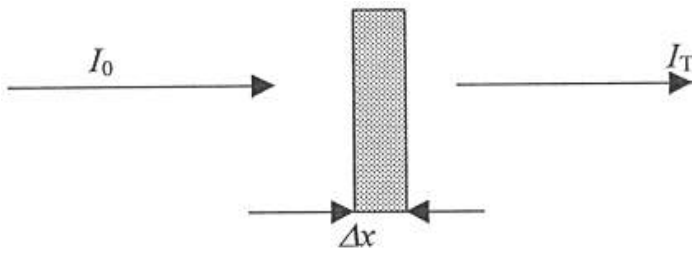

Figure 3.31**.** Absorption in a thin layer

Equation 3.7 can be written as

$$2.303\log\frac{\mathrm{I}}{\mathrm{I_0}} = -\alpha x \tag{3.10}$$

$$-log\frac{I}{I_0} = \frac{\alpha}{2.303}x \tag{3.11}$$

$$A = \varepsilon x \tag{3.12}$$

which is known as Lambert's law, where ε is the molar absorptivity and A is the absorbance or optical density (no units) which is defined as

$$A = -log\frac{I}{I_0} = -logT \tag{3.13}$$

The optical density (OD) or the absorbance (A) can also sometimes quantifies the absorption of optical mediums. It is seen from Eq.3.12 that the optical density depends on the thickness of the medium.

To find the total transmittance for a thin film, consider two regions as shown in figure

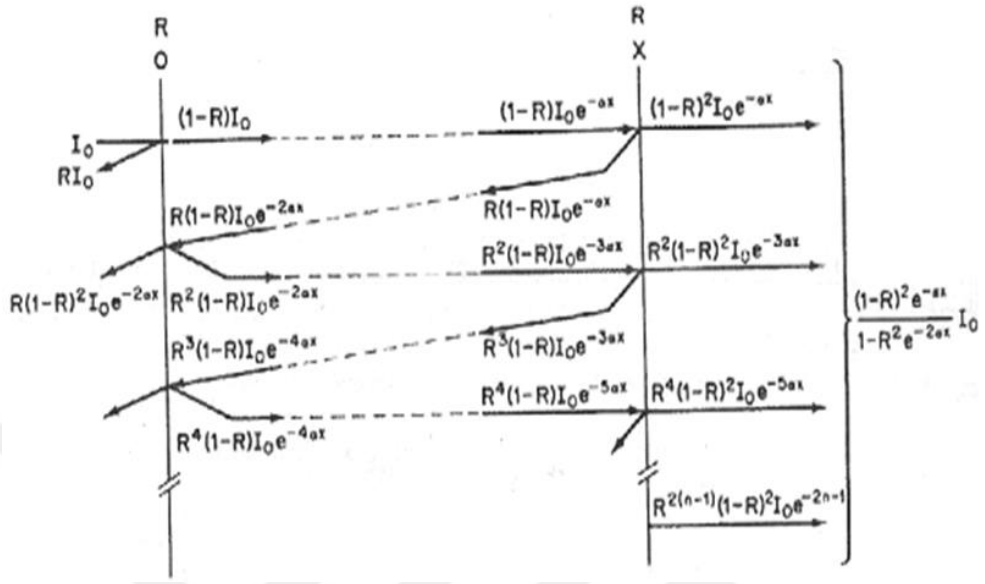

Figure 3.32. Transmission of multilayer thin film (Pankove 1975)

Neglecting the interface, assuming a monochromatic enters inside a thin film with thickness d, then the intensity of the transmitted light is

$$I = (1 - R)\, I_0$$

And the intensity of light reaching the second region takes the form

$$I = I_0\, (1 - R)\, e^{-\alpha d} \qquad (3.14)$$

The intensity of light that passes through the film is

$$I = I_0\, (1 - R)^2\, e^{-\alpha d} \qquad (3.15)$$

If the light is continued in this way, the a mount of reflected light in each reflection is

$$I = R^{2n}\, (1 - R)^2\, I_0\, e^{-(2n+1)\alpha d} \qquad (3.16)$$

The total light transmittance through the film can be written as

$$I = (1 - R)^2 I_0 e^{-\alpha d} \left(\sum_r R^{2n} e^{-2n\alpha d} \right) \quad (3.17)$$

If these internal reflections are continued as shown in the figure, the total transmittance will be

$$T = \frac{(1-R)^2 e^{-\alpha d}}{1 - R^2 e^{-2\alpha d}} \quad (3.19)$$

For large absorber region d >> 0 Eq. 3.19 becomes

$$T = (1-R)^2 e^{-\alpha d} \quad (3.20)$$

Taking the natural logarith (ln) of both sides of equation and solving for α

$$lnT = \ln[(1 - R)^2 e^{-\alpha d}] \quad (3.21)$$

$$2.3 logT = \ln(1 - R)^2 + \ln e^{-\alpha d} \quad (3.22)$$

$$-2.3A = \ln(1-R)^2 - \alpha \, \boldsymbol{d} \quad (3.24)$$

$$\alpha = \frac{1}{d}\left[2.3A + \ln(1-R)^2\right] \quad (3.25)$$

By using the Eq. 3.25, the absorption coefficient can be calculated. If we neglect the term containing the reflection value R, Eq. 3.25 becomes

$$\boldsymbol{\alpha = \frac{1}{d}(2.3A)} \quad (3.26)$$

The absorption data can be obtained from the spectrometer. The formula for calculation of absorption coefficient due to optical transmittance

$$\alpha = \frac{1}{d}\left[\ln\left(\frac{1}{T}\right)\right] \quad (3.27)$$

From the last formula we can calculate the absorption coefficient due to optical transmittance (Kara 2008).

3.3.2.2 Direct and Indirect Band Gaps

The separation region between the lowest-energy point of the conduction band and the highest-energy point of the valance band is called the "bandgap". The difference in energy between these two points is known as the "bandgap energy" and it is symbolized by Eg. The lowest point of the conduction band is known as "conduction band edge", and the highest point of the valence band is known as "valence band edge". (Kittel 2005; López, Gómez, and technology 2012)

In semiconductor materials, there are two types of bandgaps: a direct bandgap and an indirect bandgap. Each of the lowest-energy state of the conduction band and the highest-energy state of the valence band are described by a certain crystal momentum ($\vec{k}$-vector). If the ~k vectors for both states are the same, the bandgap is called "direct bandgap" (Fig. 2.3). Otherwise, it is called "indirect bandgap" (Fig. 2.4). In other words, if the momenta of electrons and holes in both valence band and conduction band are the same, the bandgap is called "direct bandgap"; in this case the photon can be directly emitted by the electron. In "indirect bandgap" the electron cannot emit a photon because it passes through an intermediate state in which electron transfers momentum to the crystal lattice.

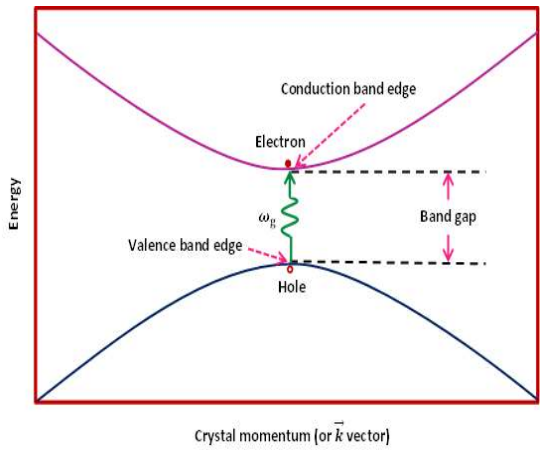

Figure 3.33. Schematic graph of energy against crystal momentum (or $\vec{k}$ vector) for a direct-bandgap semiconductor.

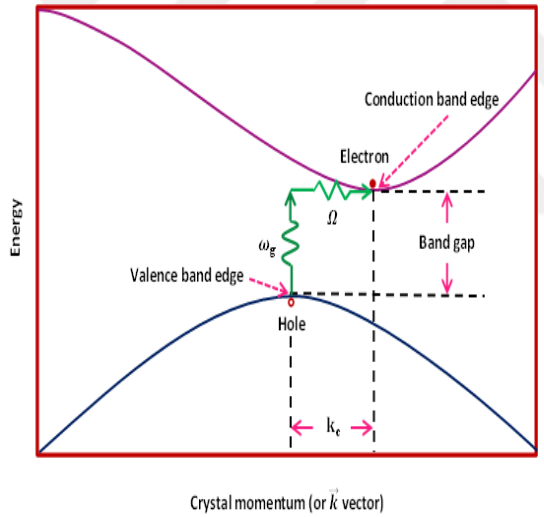

Figure 3.34. Schematic graph of energy against crystal momentum (or $\vec{k}$ vector) for an indirect-bandgap semiconductor.

3.3.2.3. Calculation of the forbidden bandgap energy

Gap energy is fundamental quantity to investigate the optical properties of material. A simple and common way for evaluating the forbidden bandgap energy Eg and to determine whether this bandgap is direct or indirect is by using the

absorption spectroscopy. By plotting a certain power of the absorption coefficient α versus photon energy (E= hν), both the bandgap energy and whether this bandgap is direct or not can be determined. The bandgap energy Eg for a semiconductor is related to optical absorption coefficient α according to the relation (Kernazhitsky et al. 2013)

$$\boldsymbol{\alpha h\nu = A_c(h\nu - E_g)^r} \quad (3.28)$$

Where $\boldsymbol{A_c}$ is a constant related to the ordered crystalline structure, and r is an exponent associated with the type of transition. Equation 3.28 is known as Tauc law, and the plot of it is known as Tauc plot. For direct allowed transitions r =$\frac{\mathbf{1}}{\mathbf{2}}$, for direct forbidden transitions r =$\frac{\mathbf{3}}{\mathbf{2}}$ and r =2 for indirect allowed ones. Plotting the relation between $(\boldsymbol{\alpha h\nu})^{\frac{1}{r}}$ as y-axis and hν as x-axis one gets the Tauc plot which defines the optical gap in amorphous semiconductors. Extending the tangent of the straight portion (at E > Eg) of $(\boldsymbol{\alpha h\nu})^{\frac{1}{r}}$ - E curve one can evaluate the bandgap energy Eg from the intersection of the tangent and the photon energy axis $\boldsymbol{h\nu}$.

3.3.2.4. Calculation of Urbach energy

The investigation of interactions among electrons, holes, photons, and phonons is one of the most important problems of crystal spectroscopy. From the measurements of absorption band shape at different temperatures, one can obtain certain information on these interactions. In many cases, the absorption coefficient at the band edge vary exponentially with the energy of light at a specific temperature. This exponential function is known as Urbach rule (Kurik 1971). In 1953, Urbach found by experiment that the absorption coefficient α varies exponentially with photon energy (E) according to the relation

$$\alpha(E) = \alpha_0 exp\left(-\frac{E_g - E}{E_U}\right) \quad (3.29)$$

where $\boldsymbol{\alpha_0}$ is the absorption coefficient at photon energy E = Eg and E_U is called Urbach energy. Taking the natural logarithm of Eq. 3.29 we obtain

$$\ln(\alpha) = \left(\ln(\alpha_0) - \frac{E_g}{E_U}\right) + \left(\frac{1}{E_U}\right) E \quad (3.30)$$

Plotting the relation between ln(α) and E, Urbach energy E_U can be calculated from the slope of the straight line (Urbach 1953). The change in the absorption coefficient of an amorphous semiconductor according to energy is shown in Figure 3.36 B region is called Urbach region or Urbach tail.

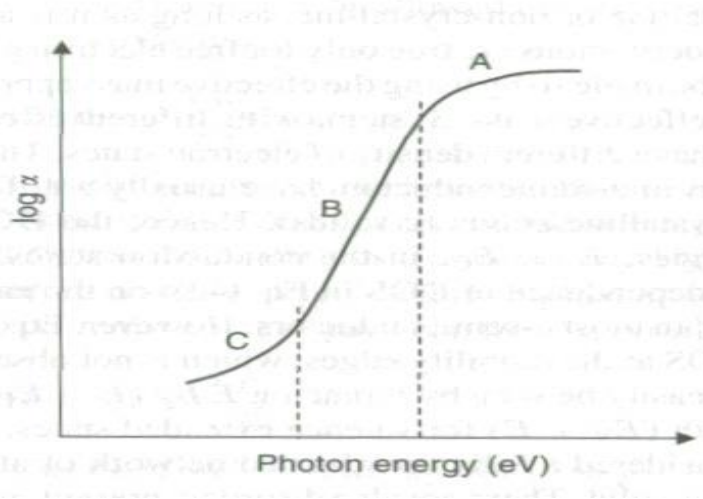

Figure 3.35. The change in the absorption coefficient of an amorphous semiconductor according to energy

3.3.3 Atomic Force Microscopy (AFM)

Gerd Binning et al, Christoph Gerber and Calvin Quate demonstrated the ideas of AFM for the first time in 1986. The atomic force microscope is a high-resolution type of scanning microscopy for studying properties of the material on a nanoscale. A 3D topographical image of the sample surface can be obtained by

measuring the force between a probe and a sample surface (Binnig, Quate, and Gerber 1986).

Figure 3.37 shows the general components of AFM and their functions. As the tip approaches the surface, the attractive force deflects the cantilever towards the surface, and when the tip is brought into contact with the sample, the repulsive force deflects the cantilever away. These deflections are detected by a laser beam. The deflection changes the reflected beam direction. A photodiode is used to register the changes.

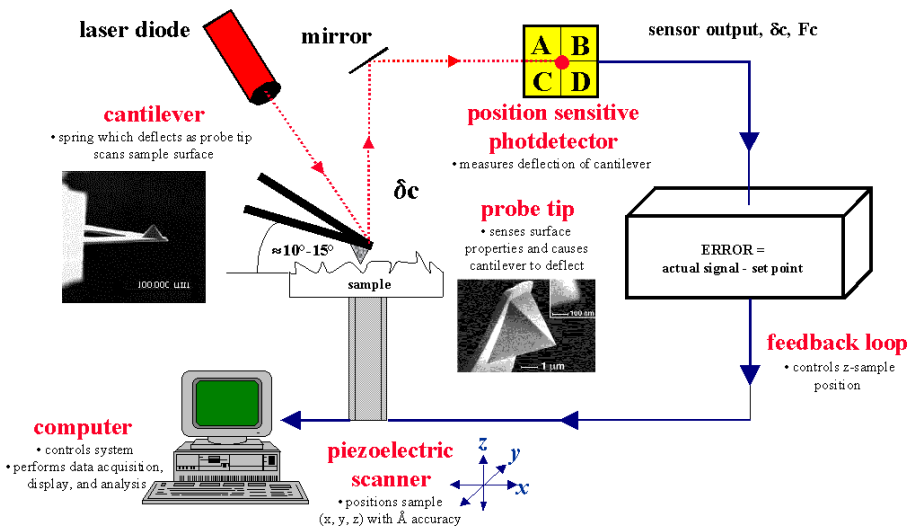

Figure 3.36. A schematic diagram for the working principle of AFM

The cantilever can be thought of as a spring. The amount of the generated force depends on the spring constant (stiffness) of the cantilever and the distance between the tip and the sample. This force can be characterized by Hooke's Law.

$$F=-kx$$

where F is the generated force, k is the spring constant and x = cantilever deflection

There are three primary imaging modes in AFM:

1. Contact mode
2. Non-contact mode
3. Intermittent (Tapping) mode

These modes are determined by the probe-surface separation. In this experiment, AFM measurements are done in non-contact mode.

Force-distance curves allow researchers to study the mechanical properties of a sample. In the non-contact region, the distance between the probe and the sample is about tens to hundreds of angstroms and the interatomic force is attractive. While in the contact region, the tip is held less than a few angstroms (10^{-10} m) from the sample surface and the repulsive force becomes dominant. The relationship between force and distance is shown in Figure 3.37 (Robert and Heather 2012).

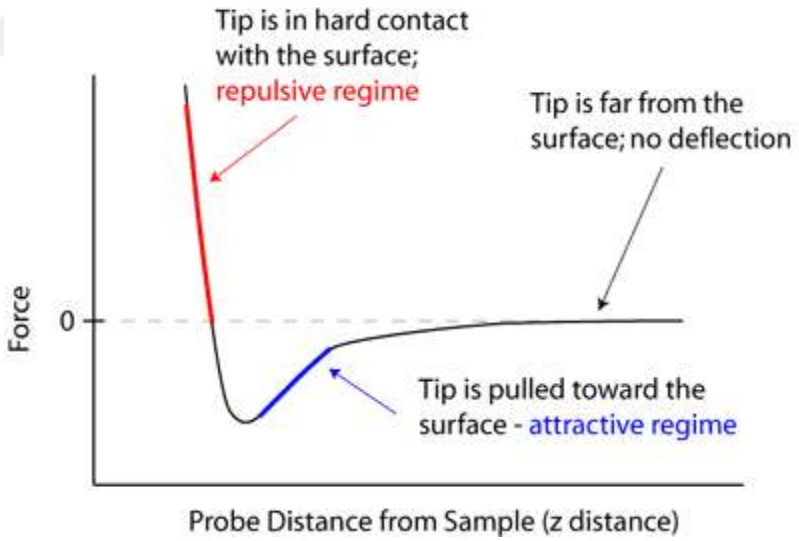

Figure 3.37. Different regions within the force curve.

3.3.4. Raman Spectroscopy

Raman spectroscopy is based on the Raman effect first reported by the Indian physicist C. V. Raman in 1928. He observed that the wavelength of a small fraction of the scattered beam by certain molecules differs from that of the incident beam. Moreover, the shifts in wavelength depend on the chemical structure of these molecules (Raman and Krishnan 1928).

Raman spectroscopy is a spectroscopic technique depends on inelastic scattering of monochromatic light, commonly from a laser source. It is one of the most important means for nanotechnology and nanoscience since it is highly sensitive to the chemical and physical properties of materials and to the effects of the environment that change these properties.

Two different scattering phenomena can occur due to light-matter interactions:

1. Rayleigh scattering: is an elastic scattering process, in which the energies of scattered and incident photons are the same (Fig. 3.38 b).
2. Raman scattering or (Raman Effect): is an inelastic scattering process which means that there is a frequency difference between the incident photon frequency and scattered photon frequency and this difference depends on the properties of the material. Anti-Stokes line (Fig. 3.38 c) is the Raman scattered light detected on the shorter wavelength reigon while Stokes line (Fig. 3.38 d) detected on the longer wavelength reigon.

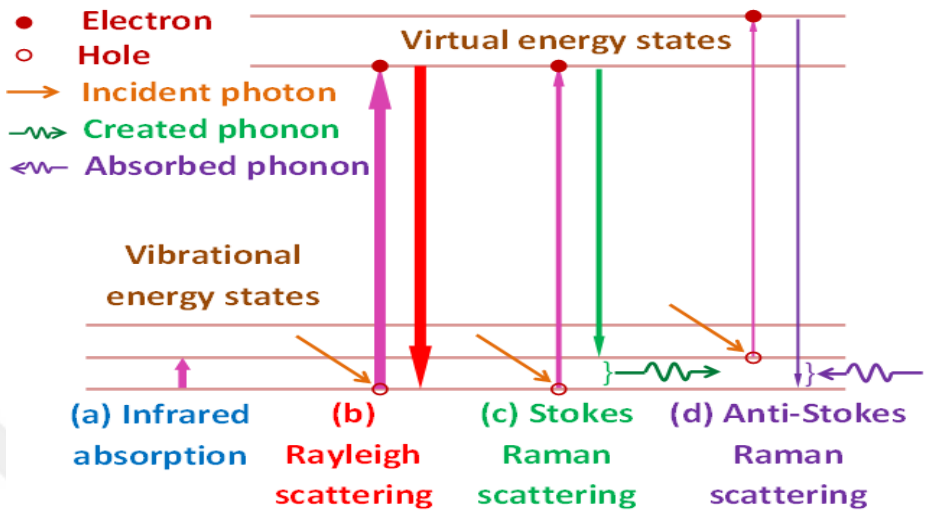

Figure 3.37. Different transitions involved in Raman spectra

Raman spectrum is a plot between the intensity of the scattered light I_s as y-axis and the change in energy of the scattered light represented by the change in frequency of scattered light, which is known as Raman shift, as x-axis. Raman shift is reported in units of wavenumber cm^{-1} and is defined by

$$Raman\ shift(cm^{-1}) = \frac{1}{\lambda_i} - \frac{1}{\lambda_s}$$

Raman spectrum shows molecular fingerprint of the target. Peak position shows the specific vibration mode of each molecular in the material. Peaks appear at a phonon energy Eq (the excitation energy associated with Raman scattering). The energy of Stokes scattering takes place at a positive value of Eq, while the anti-Stokes scattering takes place at a negative value of Eq (Figure 3.39)

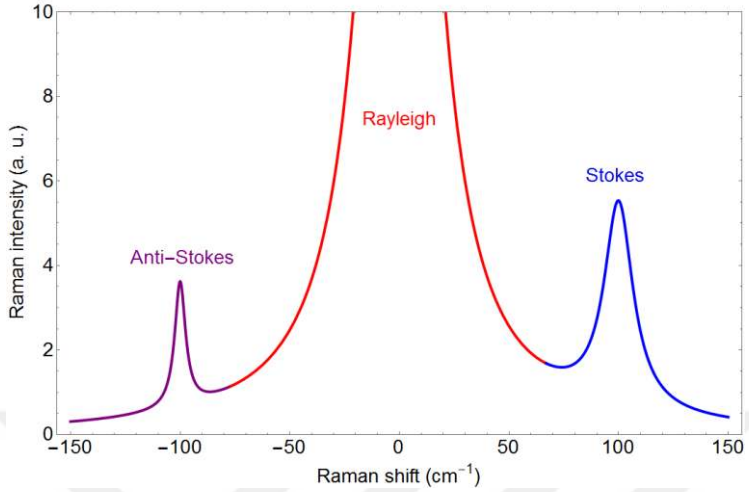

Figure 3.38. Schematic plot showing Rayleigh scattering and Raman spectrum (+ve frequency for Stokes scattering and -ve frequency for anti-Stokes).

4. RESULTS AND DISCUSSION

In this study, diamond-like carbon (DLC) and hydrogenated silicon carbide (Si_xC_y: H) films have been grown on silicon and glass substrates employing an (ECR- MP CVD) system. The substrates were cleaned firstly by immersing them in methanol at room temperature for 20 min and then washed by distilled water. They dried finally by nitrogen blowing. Microwaves with a frequency of 2.45 GHz were generated by a microwave magnetron. A magnetic field with a magnitude of 875 Gauss applied. A rotary and a turbo molecular pump were used to evacuate the deposition chamber. Before the deposition, reaction chamber was flushed with (CH_4) to remove the unwanted gas and water vapor. The flow rates were controlled by mass flow controllers. The base pressure of the deposition chamber was 10^{-7} Torr and the temperature of the substrate was held constant at 25°C.

All samples were prepared by the same (ECR) system under different conditions. They can be classified into three sets as following:

i. Six samples were deposited onto glass substrate without applying any bias to the substrate. The microwave power was held constant with varying values of working pressure. The deposition time for these samples was 30 min.

ii. Three samples (W-8, W-10, and W-11) were deposited on a biased glass substrate at different bias voltages with deposition time of 30 min.

iii. Two samples (W-12 and W-14) were deposited on Si substrate for 20 minutes. One of the substrates was biased and the other was unbiased.

Deposition on both glass and Si substrates can be seen in Figures 4.1 and 4.2. Deposition parameters for all deposited films are listed in Tables 4.1, 4.2 and

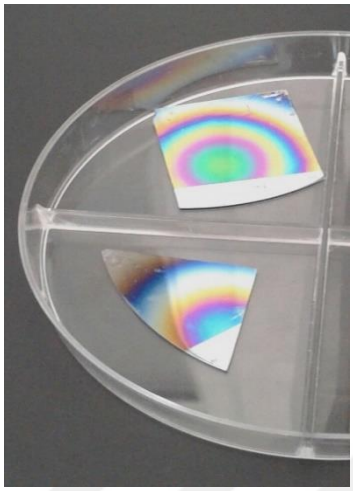

Figure 4.1. Image of deposition on Si substrates

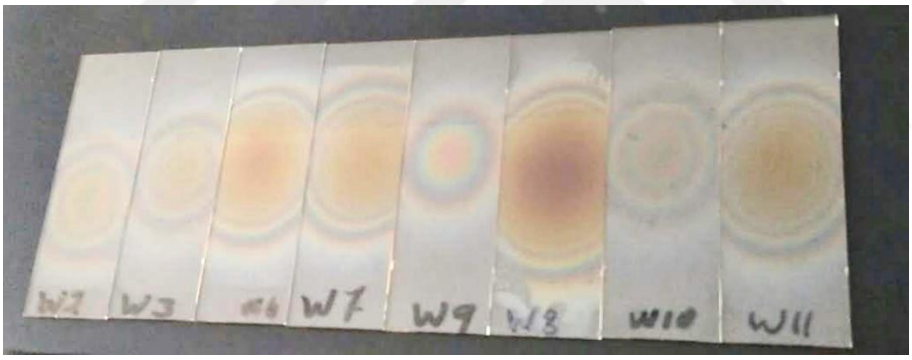

Figure 4.2. Image of deposition on glass substrates

Table 4.1. Parameters for films deposited on glass substrate under different working pressure without any external field

Microwave power = 45W			
Deposition time = 30 min			
Sample name	**Film type**	**Working Pressure (Torr)**	**CH_4 Gas Flow (sccm)**
W-2	SiC	$4x10^{-3}$	8
W-3		$4.1x10^{-3}$	8
W-4		$4.4x10^{-3}$	8
W-6	DLC	$4.5x10^{-3}$	8
W-7		$4.6x10^{-3}$	8
W-9		$4.7x10^{-3}$	8

Table 4.2. Parameters for films deposited on biased glass substrate with an external field

Working pressure = $4.5x10^{-3}$ Torr				
Deposition time = 30 min				
Sample Name	**Film type**	**Applied Voltage (V)**	**CH_4 Gas Flow (sccm)**	**Microwave power (watt)**
W-10	DLC	150	9	45
W-11	DLC	155	9	47.5
W-8	DLC	200	9	50

Table 4.3. Parameters for SiC films deposited onto Si substrate

Working pressure = $5x10^{-3}$ Torr			
Deposition time = 20 min, Temperature = 25 ◦C			
Sample Name	**CH_4 Gas Flow (sccm)**	**Microwave power (watt)**	**Applied Voltage (V)**
W-12	8	45	0
W-14	7	50	150

4.1 Optical Properties

4.1.1. Optical Properties of carbon thin films deposited on glass substrate without applying any external field

The optical properties of all the films were investigated by a double beam computer controlled spectrophotometer (Perkin Elmer Lambda 2S) in the UV/VIS/NIR regions. The optical transmittance was recorded in the wavelength range of 300–1100 nm. The plasma power was kept the same and all of these films deposited for 30 minutes only the pressure was changed. As shown in Figure 4.3 the optical transmission was found to be more than 90% in the visible region. From Table 4.4, it is noticed that the band gap energy increases with the increase of the deposition pressure. This result is in good agreement with other studies (Chen et al. 2014).

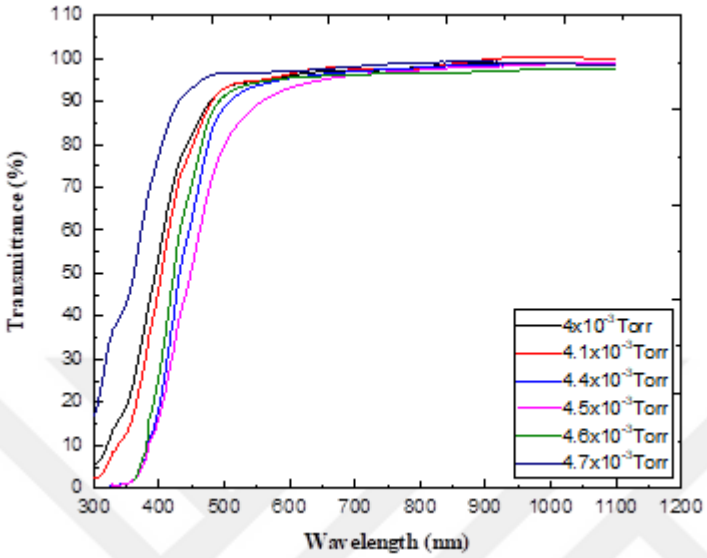

Figure 4.3. The transmittance spectra of six films produced at different working pressure of 45W microwave power.

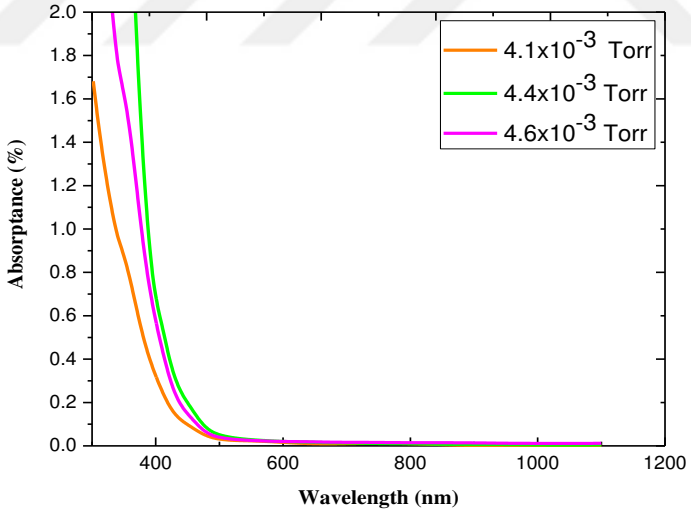

Figure 4.4. The absorption spectra of three films produced at different working pressure of 45W microwave power.

The thickness of some of these films was calculated using Eq.4.1.

$$d = \frac{\lambda_1 \lambda_2}{2(\lambda_1 n_1 - \lambda_2 n_2)} \quad (4.1)$$

where d is the thickness of the film, n_1 and n_2 are the refractive indices at two adjacent maxima (or minima) at λ_1 and λ_2. A double wavelength (530 and 632 nm) ellipsometry (TT-30) was used to find the refractive index. The band gap of the films was also calculated from the linear fit to the linear portion of the $(\alpha h\nu)^{\frac{1}{2}}$ versus $h\nu$ plot as shown in Figure 4.5. The optical band gap energies and the thickness values are tabulated in Table 4.4.

Table 4.4. Thickness (d) of W-3, W-4 and W-5 thin films

Film name	λ_1 (nm)	λ_2 (nm)	n_1	n_2	d (nm)
W-3	975	546	3.2670	3.4340	203
W-7	1004	617	2.3924	2.4119	338
W-9	876	566	3.2928	3.4237	262

Table 4.5. Band gap energy (Eg) of obtained thin films for 30 min at different values of working pressure

Film name	W-3	W-7	W-9
Working pressure (Torr)	4.1×10^{-3}	4.6×10^{-3}	4.7×10^{-3}
Eg (eV)	2.4	2.51	2.71

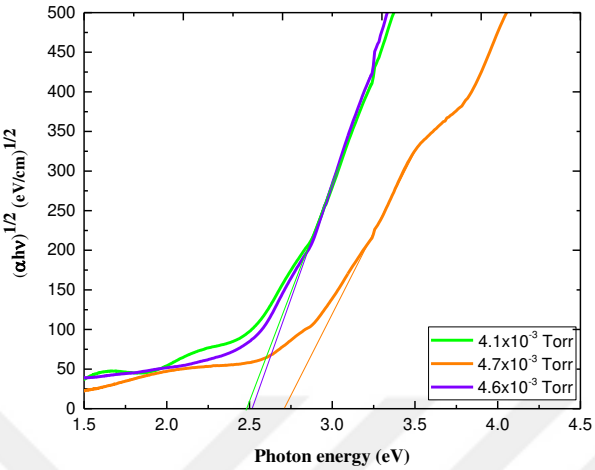

Figure 4.5. Optical energy gap determination for carbon films with different working pressure.

4.1.2. Optical properties of carbon semiconductor thin films deposited on glass substrate with applying external field

Figure 4.6 shows the transmittance versus wavelength graph for three films which deposited at different values of an external bias voltage applied to a terminal of glass substrate during the deposition process. It was observed that the presence of the electric field reduces the transmission ratio. The transmission ratio decreases as the bias voltage increases. In the visible region, the transmission was more than about 80%. In addition, the microwave power was increased from 45W to 50W.

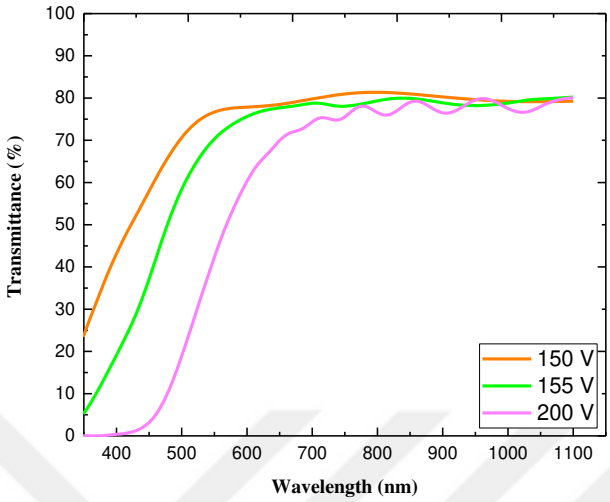

Figure 4.6. The transmittance spectra of three thin films produced at the same working pressure 4.5×10^{-3} Torr and different applied voltage.

As can be seen from in Figure 4.7 the absorption spectrum shifts toward longer wavelength as bias voltage increases

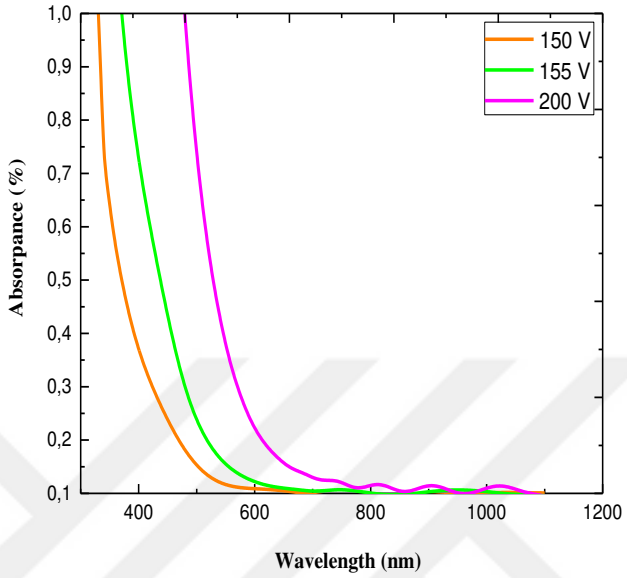

Figure 4.7. The absorption spectra of three thin films produced at different applied voltages.

Table 4.6. The band gap energy (Eg) of deposited thin films for 30 min at different values of bias voltage

Film name	W-10	W-11	W-8
Applied voltage (V)	150	155	200
Eg (eV)	2.16	2.08	1.97

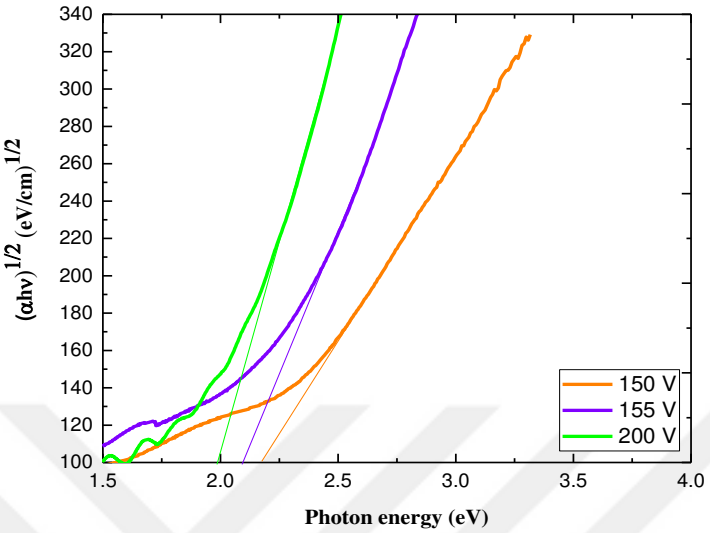

Figure 4.8. Optical energy gap determination for carbon films with different applied voltage.

The $(\alpha h\nu)^{1/2}$ versus hν plot is shown in Figure 4.8. The band gap (Eg) is found to decrease as applied voltage increases. The decrease in the band gap energy can be explained by the band gap narrowing effect (Jain and Roulston 1991; Shaker and Zekry 2010). The change in the potential between donors and the host lattice causes an increase in the doping concentration which effects on the band gap narrowing. The donor band becomes widened and overlap with the conduction band that leads to a shrinkage of the band gap (Swami et al. 2016). In addition, the band gap energy was changed as a result of different C/H ratio. The hydrogen content narrows the optical band gap from 2.16 eV to 1.97 eV for 150V and 200V biases respectively.

4.2. Raman Measurements

4.2.1. Results of Raman spectroscopy for thin films deposited on glass substrate

Raman measurements of films fabricated on glass substrates were measured with Bruker Dispersive Raman Spectrometer. The measurements of Raman scattering were conducted at room temperature in the range of 1200 cm^{-1}-1700 cm^{-1} using a laser source with a wavelength of 785 nm. Raman spectra of carbon thin films deposited at different bias voltage are shown in Figure 4.9.

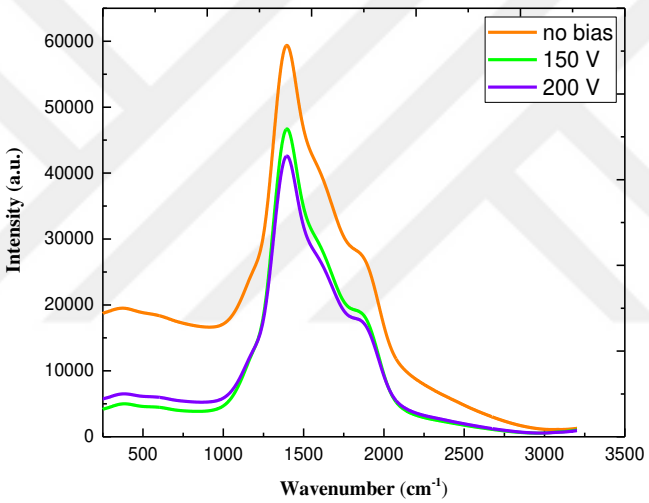

Figure 4.9. Raman spectra of carbon thin films fabricated on the glass substrates at different bias voltage.

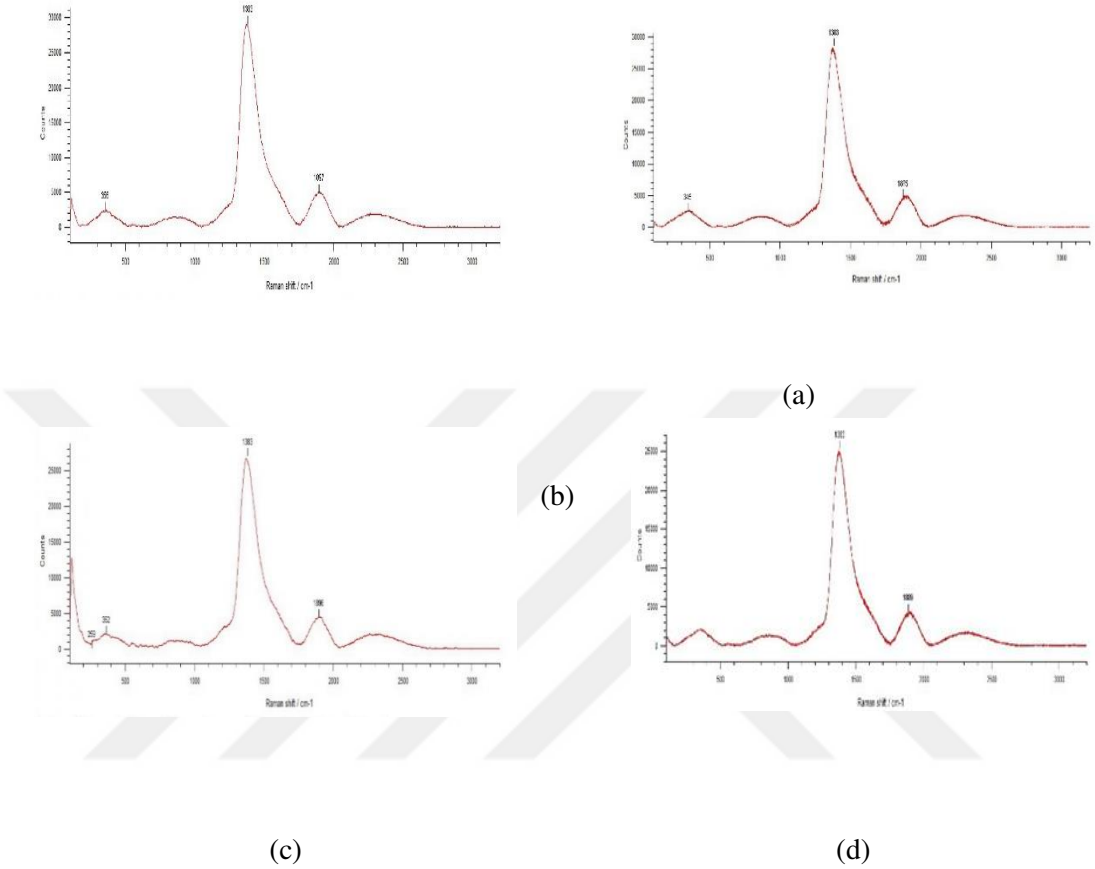

(a)

(b)

(c)

(d)

Figure 4.10. Raman spectra of carbon thin films deposited at different bias voltages: (a) unbiased, (b) 150V (c) 155V and (d) 200 V.

Raman spectra of these samples show a broad peak, ranging from about 1200 cm^{-1} to 1700 cm^{-1}. The most prominent Raman peak in sample W-8 is located at approximately 1380 cm^{-1}. The Raman spectrum is quite close to that of diamond-like carbon (DLC). Figure 4.10 gives the visible Raman spectra for all of these samples which deposited at different applied voltages. All the samples exhibit both the G and D peaks. The intensity of the peaks and Half Full width at half maximum (FWHM) are listed in Table 4.6.

Table 4.6. Peak position, half-widths and intensity obtained from Raman measurements of samples W-9, W-10 and W-11

Film name	Peak no	Center (cm^{-1})	FWHM	Intensity
W-9 (no bias)	1	355.842	148.087	2430.85
	2	1383.1	144.94	29361.2
	3	1896.97	143.8	5046.49
W-10 (150 V)	1	344.988	169.288	2630.01
	2	1382.7	141.386	28982.9
	3	1874.68	142.3	4894.16
W-11 (155 V)	1	258.548	108.754	138.594
	2	362.348	158.018	2126.15
	3	1382.73	142.771	27335
	4	1896.19	141.014	4501.72

From the results presented in Table 4.6, it can be noticed that the G peak position shifts downwards from 1896.97 to1874.68 cm^{-1} when 150V was applied. However, with increasing of the bias voltage to 155 V, the G peak position shifts upwards to 1896.19 cm^{-1}. The band shift towards lower wavenumbers indicates that there is an increase in sp^3 bonded carbon. For substrate, a bias of 150 V the sp3 bonded carbon content in the film is relatively high compared to the unbiased and 155 V biased sample. The decrease in G peak half-maximum value indicates that the samples tend to turn into a more regular graphitic structure (Dey et al. 2008; Wang et al. 2011).

4.2.2. Results of Raman spectroscopy for carbon thin films deposited on silicon substrate

The measurements of the films, which were synthesized on silicon substrates, were measured in the range of 250 cm^{-1}-3000 cm^{-1} using a laser source with a wavelength of 1064 nm. Results of Raman analysis of two SiC films are

discussed. An electrical field is applied to one of them to observe its effect during the deposition process.

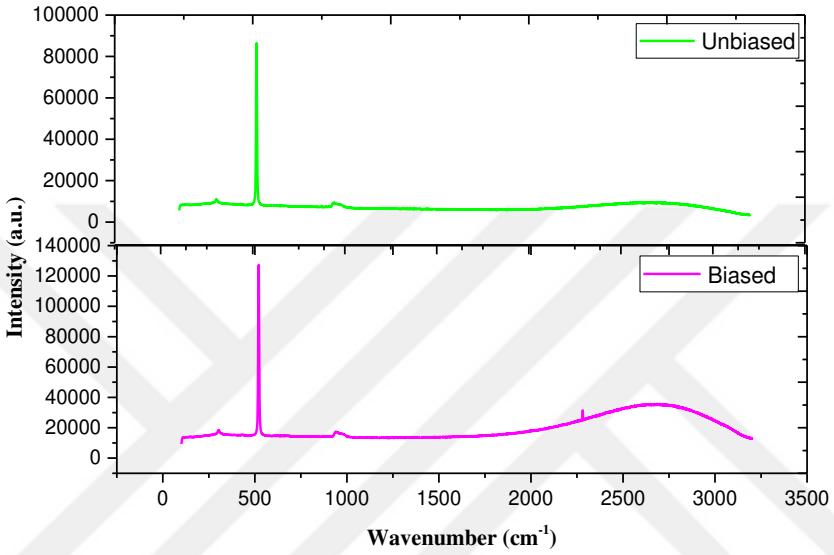

Figure 4.11. Raman spectra of SiC thin films grown on Si substrates.

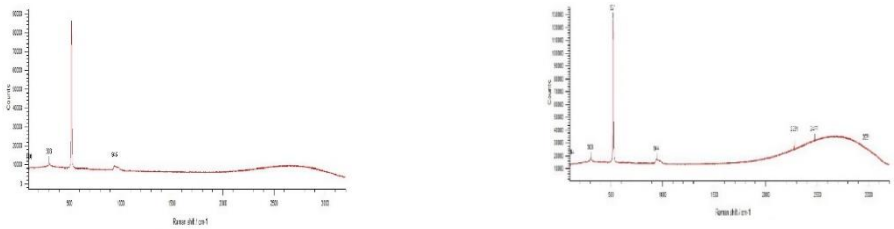

(a) (b)

Figure 4.12. Raman measurements for two SiC thin films (a) no bias (b) with 150 V bias voltage

Figures 4.11 and 4.12 show the Raman scattering spectra for SiC thin films. Referring to these figures, one can make a comparison between the two spectra. The distinct peak in both spectra is located at about 500 cm^{-1}, but the distinct peak

in the second spectrum (Fig.4.12 (b)) has a higher intensity than the other. In addition, the Raman spectrum of the film, which deposited under the bias, has more peaks.

4.3. XRD Results

The nanocrystal structure of two SiC thin films was characterized by powder X-ray diffraction pattern using Rigaku Miniflex II X-ray Diffractometer with Cu Kα radiation (λ=1.54059A^0) with scan speed 0.4^0/min. X-ray diffraction spectra of SiC thin film samples are shown in Figure 4.13.

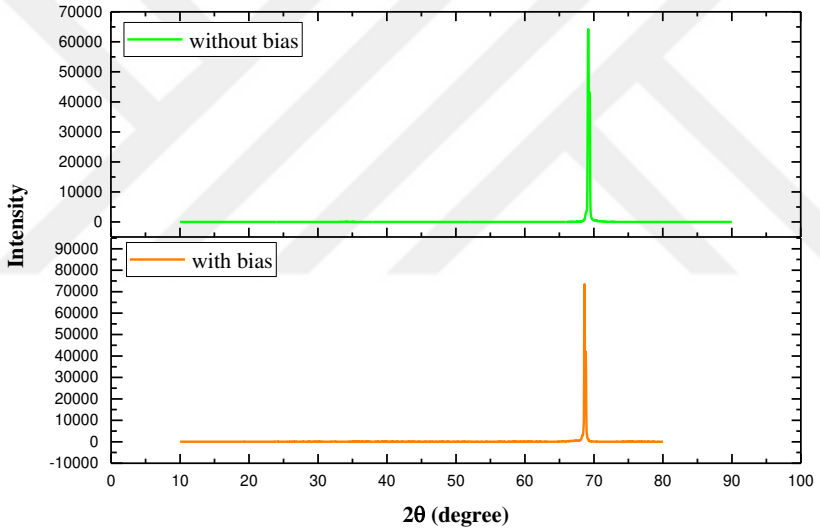

Figure 4.13. XRD pattern for SiC thin films

Table 4.7. Intensity, FWHM and grain size obtained from XRD analysis.

Film name	Applied voltage (V)	Diffraction angle 2θ (degree)	Distance between Planes d (A)	Intensity	FWHM	Grain Size (nm)
W-12	0	69.114	1.35667	65116.48	0.147	687
W-14	150	68.763	1.36351	73987.45	0.120	392

As it is evident from X-ray diffraction spectra in Fig.4.13 and from Table 4.7, the intensity of the prominent peak became stronger when bias was applied to the substrate. Thus, denote that the substrate biasing can improve the crystallinity of the thin films. The deposited film shows more ordered structure. The grain size decreases by applying a bias voltage. This result is in good agreement with a previous study on TiO_2 thin film (Bait et al. 2017). The possible reasons are the penetration of ions into the condensed film. Substrate bias can cause resputtering of species from the produced film surface. As a result of this grain size gets smaller (Adochite et al. 2012).

4.4 Atomic Force Microscopy (AFM) Results

Atomic force microscopy (AFM) on a Park XE 70 AFM system in non-contact mode was used to analyze the surface topography of samples. Figure 4.14 shows 3D AFM images of the films fabricated on glass substrates.

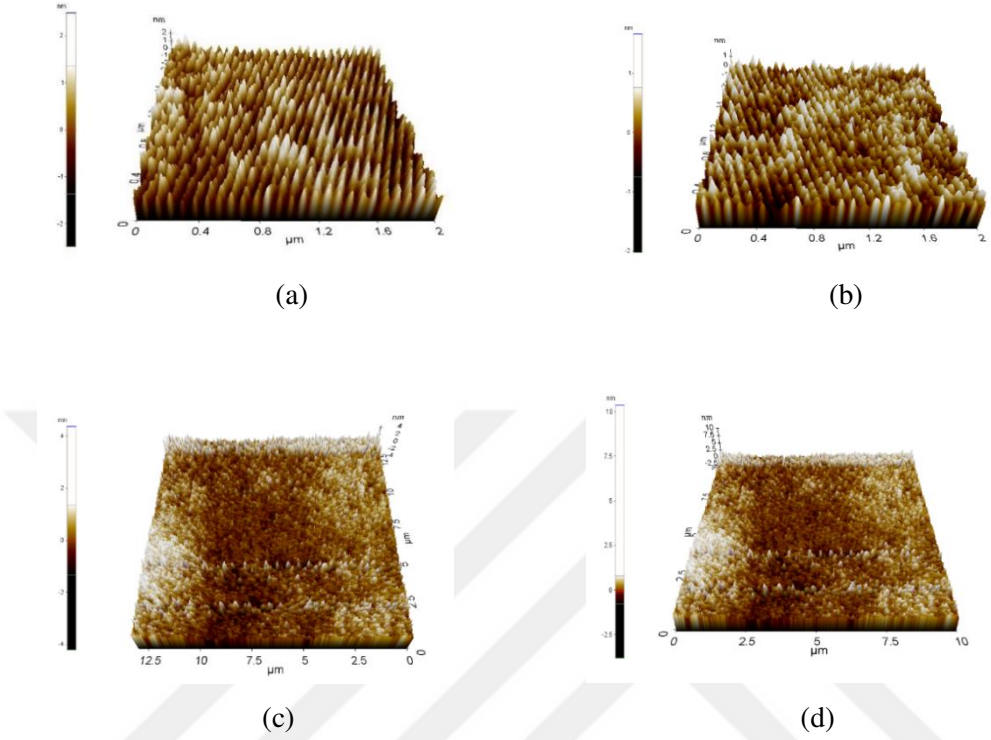

(a) (b)

(c) (d)

Figure 4.14. AFM 3D images of carbon films (a), (b) unbiased (c), (d) biased

It can be seen from Fig.4.15 that the carbon film layer is properly coated on the surface and there is no gap. In addition, the unbiased deposited films are relatively smooth and uniform as compared to biased films. The films deposited at a bias voltage show many areas with different sizes distributed randomly on the film surface that is imputed to the intense, energetic ion bombardment on the growing surfaces (Wang et al. 2011).

5. CONCLUSION

In this work, carbon films produced from the methane gas using ECR system. In thin films ≈100-300 nm silicon carbide films obtained for the first time. Si contribution comes from the substrate which is soda-lime glass. So the obtained films can be denoted as Si_xC_y:H, to emphasize that the composed films are not stoichiometric and contain hydrogen. With this configuration, a thin layer of SiC formed at the surface of the Si crystal substrate. Thicker films (>300 nm) do not contain SiC as expected. Since Si atoms cannot reach the film formation layer. Raman spectra of these films are similar to those of DLC films.

This study investigates the effect of an external electric field on the properties of producing films. Spectrophotometer, X-ray diffraction and Raman spectroscopies were used to investigate the optical and structural properties of the films. The morphological properties of the films were determined by AFM analysis. The results can be summarized as follows:

- Bias voltages affect the film formation; since in any plasma containing CH_4 we expect to have CH, CH_2 and CH_3 in large quantities. C and H ions with different charge/mass ratios resulting in different C/H film regions. This C/H ratio narrowed the optical energy gaps of the films, from 2.16 eV to 1.97 eV for 150V and 200V biases respectively. As mentioned in the section 4.1.2 this narrowing effect comes shallow when the donor band overlaps with the conduction band. While the microwave power increased from 45W to 50W.
- The Eg values of films grown at different working pressure were estimated as 2.4, 2.51 and 2.71 eV, respectively. It was indicated that the band gap was increased by increasing the deposition pressure.
- The optical transmission of all samples that deposited on glass substrate without applying any external field was found to be more than 90% in the visible region, but for samples deposited with applying external field was

found to be around 80%. This means that the presence of the electric field reduces the transmission ratio.

- Raman spectra of the samples deposited on glass substrate show a high peak in the range of about 1200 cm^{-1} to 1600 cm^{-1}. A high peak is located at approximately 500 cm^{-1} in Raman spectra of the samples grown on Si substrate.
- The sp^3 bonded carbon content in 150V biased film is relatively high compared to the unbiased and 155 V biased films. As bias voltage increased, the samples tend to turn into a more regular graphitic structure.
- XRD studies show that applying a bias voltage results more crystalline film. The deposited film shows a more ordered structure. From AFM results, it was observed that the unbiased deposited films are relatively smooth and uniform as compared to biased films.

REFERENCES

Adochite, RC, D Munteanu, M Torrell, L Cunha, E Alves, NP Barradas, A Cavaleiro, JP Riviere, E Le Bourhis, and D %J Applied Surface Science Eyidi. 2012. 'The influence of annealing treatments on the properties of Ag: TiO2 nanocomposite films prepared by magnetron sputtering', 258: 4028-34.

Andres, RP, Robert S Averback, WL Brown, LE Brus, WA Goddard, A Kaldor, SG Louie, M Moscovits, PS Peercy, and SJ %J Journal of Materials Research Riley. 1989. 'Research opportunities on clusters and cluster-assembled materials—A Department of Energy, Council on Materials Science Panel Report', 4: 704-36.

Bait, L, L Azzouz, N Madaoui, and N %J Applied Surface Science Saoula. 2017. 'Influence of substrate bias voltage on the properties of TiO2 deposited by radio-frequency magnetron sputtering on 304L for biomaterials applications', 395: 72-77.

Bewilogua, Klaus, Dieter %J Surface Hofmann, and Coatings Technology. 2014. 'History of diamond-like carbon films—from first experiments to worldwide applications', 242: 214-25.

Binnig, Gerd, Calvin F Quate, and Ch %J Physical review letters Gerber. 1986. 'Atomic force microscope', 56: 930.

Brezeanu, G. 2005. "Silicon carbide (SiC): a short history. an analytical approach for SiC power device design." In *CAS 2005 Proceedings. 2005 International Semiconductor Conference, 2005.*, 345-48. IEEE.

Casiraghi, C, AC Ferrari, and J %J Physical Review B Robertson. 2005. 'Raman spectroscopy of hydrogenated amorphous carbons', 72: 085401.

Charitidis, CA %J International Journal of Refractory Metals, and Hard Materials. 2010. 'Nanomechanical and nanotribological properties of carbon-based thin films: a review', 28: 51-70.

Chen, Jing Wei, Lei Zhao, Hong Wei Diao, Su Zhou, Ge Wang, and Wen Jing Wang. 2014. "Effect of Deposition Pressure on the Properties of Silicon Thin Films." In *Advanced Materials Research*, 70-73. Trans Tech Publ.

Cogan, Stuart F, David J Edell, Andrew A Guzelian, Ying Ping Liu, Robyn %J Journal of Biomedical Materials Research Part A: An Official Journal of The Society for Biomaterials Edell, The Japanese Society for Biomaterials,, The Australian Society for Biomaterials, and the Korean Society for Biomaterials. 2003. 'Plasma- enhanced chemical vapor deposited silicon carbide as an implantable dielectric coating', 67: 856-67.

Cui, J, Rusli, SF Yoon, EJ Teo, MB Yu, K Chew, J Ahn, Q Zhang, T Osipowicz, and F %J Journal of Applied Physics Watt. 2001. 'Effect of radio-frequency bias voltage on the optical and structural properties of hydrogenated amorphous silicon carbide', 89: 6153-58.

Delhaes, Pierre. 2013. *Carbon-based solids and materials* (John Wiley & Sons).

Dey, RM, SB Singh, A Biswas, RB Tokas, N Chand, S Venkateshwaran, D Bhattacharya, NK Sahoo, SW Gosavi, and SK %J Current Applied Physics Kulkarni. 2008. 'Substrate bias effects during diamond like carbon film deposition by microwave ECR plasma CVD', 8: 6-12.

Durand-Drouhin, O, M Lejeune, and M %J Journal of applied physics Benlahsen. 2002. 'Growth and bonding structure of hard hydrogenated amorphous carbon thin films deposited from an electron cyclotron resonance plasma', 91: 867-73.

Fecht, Hans J, and Kai Brühne. 2016. *Carbon-based nanomaterials and hybrids: synthesis, properties, and commercial applications* (Pan Stanford).

FOLEA, Milena, Adriana ROMAN, and Nouraş-Barbu %J Academic journal of manufacturing engineering LUPULESCU. 2010. 'An overview of DLC coatings on cutting tools performance', 8: 30.

Gotzmann, G, J Beckmann, C Wetzel, B Scholz, U Herrmann, J %J Surface Neunzehn, and Coatings Technology. 2017. 'Electron-beam modification of DLC coatings for biomedical applications', 311: 248-56.

Guo, Jianhui, Jingwei Zhang, Chuang Zhao, Jiwei Zhang, and Zhijun %J Applied Surface Science Zhang. 2011. 'Influence of temperature on structure as well as adhesion and friction and wear behavior of hydrogenated carbon nitride films prepared on silicon substrate', 258: 791-99.

Gupta, RK, Ahmed A Al-Ghamdi, F El-Tantawy, WA Farooq, and F %J Materials Letters Yakuphanoglu. 2014. 'Novel photosensor based on carbon nitride thin films', 134: 149-51.

Hao, Junying, Tao Xu, and Weimin %J Journal of non-crystalline solids Liu. 2005. 'Effect of deposition pressure on microstructure and properties of hydrogenated carbon nitride films prepared by DC-RF-PECVD', 351: 3671-76.

Harris, Gary Lynn. 1995. *Properties of silicon carbide* (Iet).

Hopper, AP, JM Dugan, AA Gill, EM Regan, JW Haycock, S Kelly, PW May, F %J Materials Science Claeyssens, and Engineering: C. 2016. 'Photochemically modified diamond-like carbon surfaces for neural interfaces', 58: 1199-206.

Huang, Xiaohua, and Mostafa A %J Alexandria journal of medicine El-Sayed. 2011. 'Plasmonic photo-thermal therapy (PPTT)', 47.

Inaba, H, S Fujimaki, K Furusawa, and S %J Vacuum Todoroki. 2002. 'ECR-plasma parameters and properties of thin DLC films', 66: 487-93.

Jain, SC, and DJ %J Solid-State Electronics Roulston. 1991. 'A simple expression for band gap narrowing (BGN) in heavily doped Si, Ge, GaAs and GexSi1− x strained layers', 34: 453-65.

Jameel, Dler Adil %J International Journal of Modern Physics, and Applications. 2015. 'Thin film deposition processes', 1: 193-99.

Jian, Sheng-Rui, Te-Hua Fang, and Der-San %J Journal of non-crystalline solids Chuu. 2004. 'Nanoindentation investigation of amorphous hydrogenated carbon thin films deposited by ECR-MPCVD', 333: 291-95.

Kano, Makoto. 2015. 'Overview of DLC-coated engine components.' in, *Coating Technology for Vehicle Applications* (Springer).

Kara, K. 2008. 'Atmalı Filtreli Katodik Vakum Ark Depolama Yöntemi İle P-tipi ZnO (Çinko Oksit) Üretimi ve Yapısal Özellikleri, Çukurova Üniversitesi Fen Bilimleri Enstitüsü', Yüksek Lisans Tezi.

Karthik, PS, AL Himaja, and Surya Prakash %J Carbonlett Singh. 2014. 'Carbon-allotropes: synthesis methods, applications and future perspectives', 15: 219-37.

Kawai, S, T Shinagawa, M Noda, M %J Diamond Umeno, and Related Materials. 2008. 'Photoconductivity of DLC film deposited by pulsed discharge plasma CVD', 17: 676-79.

Kernazhitsky, L, V Shymanovska, T Gavrilko, V Naumov, and V %J Ukrainian journal of physical optics Kshnyakin. 2013. 'Optical absorption of polydisperse TiO2: Effect of surface doping by transition metal cations': 15-23.

Kittel, C. 2005. "Int. to Solid State Physics, 8th edn., Maruzen." In.: John Wiley & Sons, Inc., New York.

Kleinsorge, B, SE Rodil, George Adamopoulos, J Robertson, D Grambole, W %J Diamond Fukarek, and related materials. 2001. 'Hydrogen and disorder in diamond-like carbon', 10: 965-69.

Klyui, NI, VG Litovchenko, AG Rozhin, VN Dikusha, M Kittler, W %J Solar energy materials Seifert, and solar cells. 2002. 'Silicon solar cells with antireflection diamond-like carbon and silicon carbide films', 72: 597-603.

Kugler, S. "Lectures on Amorphous Semiconductors, Optical Properties." In.

Kurik, MV %J physica status solidi. 1971. 'Urbach rule', 8: 9-45.

Lee, Huijea, Seong Bong Kim, Changho Yi, Seungil Park, Suk Jae Yoo, Moohyun Cho, Won %J Plasma Sources Science Namkung, and Technology. 2015. 'Electron cyclotron resonance plasma source with belt-type magnet assembly and slit antennas', 24: 015031.

Lei, YM, YH Yu, CX Ren, SC Zou, DH Chen, SP Wong, and IH %J Thin Solid Films Wilson. 2000. 'Compositional and structural studies of DC magnetron sputtered SiC films on Si (111)', 365: 53-57.

Liang, Xiaoyang, Xu Chen, Zhiqiang Li, Gang Li, Jingwei Chen, Lin Yang, Kai Shen, Ying Xu, and Yaohua %J Applied Physics A Mai. 2019. 'Effect of deposition pressure on the properties of magnetron sputtering-deposited Sb 2 Se 3 thin-film solar cells', 125: 381.

Litovchenko, VG, NI %J Solar energy materials Klyui, and solar cells. 2001. 'Solar cells based on DLC film–Si structures for space application', 68: 55-70.

López, Rosendo, Ricardo %J Journal of sol-gel science Gómez, and technology. 2012. 'Band-gap energy estimation from diffuse reflectance measurements on sol–gel and commercial TiO 2: a comparative study', 61: 1-7.

Maegawa, S, T Hasebe, Y Yamato, K Bito, S Nagashima, T Hayashi, T Mine, T Matsumoto, A Hotta, T %J Diamond Suzuki, and Related Materials. 2016. 'Time course analysis of antithrombogenic properties of fluorinated diamond-like carbon coating determined via accelerated aging tests: Quality control for medical device commercialization', 70: 33-38.

Matějka, Vlastimil, Yafei Lu, Long Jiao, Li Huang, Gražyna Simha Martynková, and Vladimír %J Tribology International Tomášek. 2010. 'Effects of silicon carbide particle sizes on friction-wear properties of friction composites designed for car brake lining applications', 43: 144-51.

Mattox, Donald M. 2010. *Handbook of physical vapor deposition (PVD) processing* (William Andrew).

Mohan Gokhale, Madhura, and Rakesh %J Mini-Reviews in Organic Chemistry Ravindra Somani. 2015. 'Fullerenes: Chemistry and its Applications', 12: 355-66.

Muguruma, Takeshi, Masahiro Iijima, William A Brantley, and Itaru %J The Angle Orthodontist Mizoguchi. 2011. 'Effects of a diamond-like carbon coating on the frictional properties of orthodontic wires', 81: 141-48.

Pal'Yanov, Yu N, AG Sokol, Yu M Borzdov, AF Khokhryakov, and NV %J Nature Sobolev. 1999. 'Diamond formation from mantle carbonate fluids', 400: 417.

Pankove, Jacques I. 1975. *Optical processes in semiconductors* (Courier Corporation).

Paul, R, R Bhar, and AK %J Materials Research Bulletin Pal. 2010. 'Field emission properties of composite nano-Au/DLC films prepared by CVD technique', 45: 576-83.

Raman, Chandrasekhara Venkata, and Kariamanikkam Srinivasa %J Nature Krishnan. 1928. 'A new type of secondary radiation', 121: 501.

Ren, Zhifeng, Yucheng Lan, and Yang Wang. 2012. *Aligned carbon nanotubes: physics, concepts, fabrication and devices* (Springer Science & Business Media).

Robert, AW, and AB %J Department of Chemistry Heather, Northern Kentucky University, Highland Heights, KY. 2012. 'Basic Theory Atomic Force Microscopy (AFM)', 41099.

Robertson, Gordon L. 2005. *Food packaging: principles and practice* (CRC press).

Robertson, John %J Materials science, and engineering: R: Reports. 2002. 'Diamond-like amorphous carbon', 37: 129-281.

Roy, M. 2017. 'Protective Hard Coatings for Tribological Applications.' in, *Materials Under Extreme Conditions* (Elsevier).

Sanchez, NA, C Rincon, G Zambrano, H Galindo, and P %J Thin Solid Films Prieto. 2000. 'Characterization of diamond-like carbon (DLC) thin films prepared by rf magnetron sputtering', 373: 247-50.

Schmidt, H, ER Fotsing, G Borchardt, R Chassagnon, S Chevalier, and M %J Applied Surface Science Bruns. 2005. 'Crystallization kinetics of amorphous SiC films: Influence of substrate', 252: 1460-70.

Schmuki, P. 2001. "Pits and Pores II: Formation, Properties, and Significance for Advanced Materials: Proceedings of the International Symposium." In.: The Electrochemical Society.

Schwarz, Florian P, Irmgard Hauser-Gerspach, Tuomas Waltimo, Bernd %J Surface Stritzker, and Coatings Technology. 2011. 'Antibacterial properties of silver containing diamond like carbon coatings produced by ion induced polymer densification', 205: 4850-54.

Sha, ZD, XM Wu, and LJ %J Vacuum Zhuge. 2005. 'Structure and photoluminescence properties of SiC films synthesized by the RF-magnetron sputtering technique', 79: 250-54.

Shaker, Ahmed, and Abelhalim %J J. Electron Devices Zekry. 2010. 'A new and simple model for plasma-and doping-induced band gap narrowing', 8: 293-99.

Shirakura, Akira, Masaki Nakaya, Yoshinori Koga, Hideyuki Kodama, Terumitsu Hasebe, and Tetsuya %J Thin Solid Films Suzuki. 2006. 'Diamond-like carbon films for PET bottles and medical applications', 494: 84-91.

Stamate, Marius D %J Applied Surface Science. 2001. 'Strong dependence of IR absorption in a-SiC: H dc magnetron sputtered thin films on H2 partial pressure', 172: 47-50.

Swami, Sanjay Kumar, Neha Chaturvedi, Anuj Kumar, Viresh %J Progress in Photovoltaics: Research Dutta, and Applications. 2016. 'Effects of electric field during deposition on spray deposited indium- doped zinc oxide films', 24: 74-82.

Tyagi, AK, and Srikumar Banerjee. 2017. *Materials Under Extreme Conditions: Recent Trends and Future Prospects* (Elsevier).

Urbach, Franz %J Physical Review. 1953. 'The long-wavelength edge of photographic sensitivity and of the electronic absorption of solids', 92: 1324.

Wang, Yongjun, Hongxuan Li, Li Ji, Fei Zhao, Qinghua Kong, Yongxia Wang, Xiaohong Liu, Weilong Quan, Huidi Zhou, Jianmin %J Surface Chen, and Coatings Technology. 2011. 'Microstructure, mechanical and tribological properties of graphite-like amorphous carbon films prepared by unbalanced magnetron sputtering', 205: 3058-65.

Yang, ZW, SH Han, TL Yang, Lina Ye, DH Zhang, HL Ma, and CF %J Thin Solid Films Cheng. 2000. 'Bias voltage dependence of properties for depositing transparent conducting ITO films on flexible substrate', 366: 4-7.

Yeo, Reuben Jueyuan. 2017. *Ultrathin Carbon-Based Overcoats for Extremely High Density Magnetic Recording* (Springer).

Zhang, Wei, Akihiro Tanaka, Koichiro Wazumi, Yoshinori %J Diamond Koga, and related materials. 2002. 'Structural, mechanical and tribological properties of diamond-like carbon films prepared under different substrate bias voltage', 11: 1837-44.

Zhou, Ji-cheng, and Xu-qiang %J Transactions of Nonferrous Metals Society of China Zheng. 2007. 'Structure and electronic properties of SiC thin-films deposited by RF magnetron sputtering', 17: 373-77.

CURRICULUM VITAE

She was born in Sudan on 15/12/1991. She completed her primary, secondary and high school education in Palestine. She graduated from Islamic University of Gaza, Faculty of Science, Department of Physics in 2013 and in the same year she worked as an assistant teacher at the Islamic University. In 2015, she graduated from Al-Quds Open University of Gaza, Higher education teacher training and worked at the ministry of education as a trainee. In the year of 2016, In the year of 2016 she was accepted in the Turkish scholarship programme to peruse her studies in Çukurova University in the department of Physics to have her master degree in Physics.